République Algérienne Démocratique et Populaire

الجمهورية الجزائرية الديمقراطية الشعبية

Ministère de l'Enseignement Supérieur et de la Recherche Scientifique

وزارة التعليم العالي والبحث العلمي

المدرسة الوطنية المتعددة التقنيات
Ecole Nationale Polytechnique

École Nationale Polytechnique

Département de Métallurgie

Schlumberger

End-of-study project dissertation

For Obtaining the State Engineer's Degree in Material's Engineering

Characterization and wear resistance analysis of thrust pins and inserts in high-speed drilling motors: optimizing performance via steel grade substitution.

Realized by:

BENARBIA Achouak

BERTAL Sarra

Supervised by :

Pr.ABADLI Kamel (ENP)

Publicly defended on July 10th 2023, in front of the jury composed of:

Pr.DAIMELLAHAbderrahmane	ENP	- President
Dr.SEDJAL Hamid	ENP	- Evaluator

ENP 2023

République Algérienne Démocratique et Populaire

الجمهورية الجزائرية الديمقراطية الشعبية

Ministère de l'Enseignement Supérieur et de la Recherche Scientifique

وزارة التعليم العالي والبحث العلمي

المدرسة الوطنية المتعددة التقنيات
Ecole Nationale Polytechnique

École Nationale Polytechnique

Département de Métallurgie

Schlumberger

End-of-study project dissertation

For Obtaining the State Engineer's Degree in Material's Engineering

Characterization and wear resistance analysis of thrust pins and inserts in high-speed drilling motors: optimizing performance via steel grade substitution.

Realized by:

BENARBIA Achouak

BERTAL Sarra

Supervised by :

Pr.ABADLI Kamel (ENP)

Publicly defended on July 10th 2023, in front of the jury composed of:

Pr.DAIMELLAHAbderrahmane	ENP	- President
Dr.SEDJAL Hamid	ENP	- Evaluator

ENP 2023

République Algérienne Démocratique et Populaire

الجمهورية الجزائرية الديمقراطية الشعبية

Ministère de l'Enseignement Supérieur et de la Recherche Scientifique

وزارة التعليم العالي والبحث العلمي

المدرسة الوطنية المتعددة التقنيات
Ecole Nationale Polytechnique

École Nationale Polytechnique

Département de Métallurgie

Schlumberger

Mémoire de projet de fin d'études

Pour l'obtention du diplôme d'ingénieur d'état en Génie des Matériaux

Caractérisation et analyse de la résistance à l'usure des goupilles de poussée et des inserts dans les moteurs de forage haute vitesse : optimisation des performances par substitution de l'acier.

Réalisé par :

BENARBIA Achouak

BERTAL Sarra

Encadré par :

Pr.ABADLI Kamel (ENP)

Soutenu publiquement le 10 Juillet 2023, Devant le jury composé de :

Pr.DAIMELLAHAbderrahmane	ENP	- Président
Dr.SEDJAL Hamid	ENP	- Examinateur

ENP 2023

ملخص

مقاومة التآكل عامل حاسم في التطبيقات الصناعية، ولا سيما في صناعة النفط والغاز، حيث يمكن أن تؤثر بشكل كبير على تكاليف الصيانة وكفاءة التشغيل. تركز هذه الدراسة على تحليل مقاومة التآكل لدبوس الدفع والمدخل في محركات الحفر عالية السرعة. تتمثل المرحلة الأولى في توصيفها باستخدام تقنيات مختلفة يمكن أن تحدد صنف الفولاذ الخاص بها، حيث تم تحديد دبوس الدفع بأنه مصنوع من الفولاذ ايSي ٩٣١٤ والمدخل بأنه مصنوع من الفولاذ ايSي ٩٣١٠. المرحلة الثانية تتضمن استكشاف آليات التآكل باستخدام جهاز اختبار الترايبومتر ثم تقييم سلوك التآكل باستخدام البروفيلومتر والمجهر الإلكتروني الماسح المتكامل مع تحليل الطاقة المنتشرة (يDS). المرحلة الأخيرة تهدف إلى تحسين أداء دبوس الدفع والمدخل من خلال استبدال فولاذ ايSي ٩٣١٠ بفولاذ ايSي ٤٣٣٧ بعد اختبار مقاومة التآكل باستخدام التقنيات نفسها المذكورة سابقا و في نفس الظروف.

الكلمات المفتاحية

دبوس الدفع والمدخل، ترايبومتر، مقاومة التآكل

Résumé

La résistance à l'usure est un facteur critique dans les applications industrielles, en particulier dans l'industrie pétrolière et gazière, où elle peut avoir un impact significatif sur les coûts de maintenance et l'efficacité opérationnelle. Cette étude se concentre sur l'analyse de la résistance à l'usure des broches de poussée et des inserts dans les moteurs de forage à grande vitesse. La première étape consiste à les caractériser à l'aide de différentes techniques afin d'identifier les nuances d'acier, qui s'avère être de l'acier AISI 9314 pour la broche de poussée et de l'acier AISI 9310 pour l'insert de poussée. La deuxième étape consiste à étudier les mécanismes d'usure en utilisant un tribomètre, puis à évaluer leur comportement d'usure à l'aide d'un profilomètre et d'un microscope électronique à balayage (MEB) intégré à un spectromètre à dispersion d'énergie (EDS). La dernière étape vise à améliorer les performances de la broche de poussée et de l'insert en remplaçant l'acier AISI 9310 par de l'acier AISI 4337, après avoir testé la résistance à l'usure en utilisant les mêmes techniques mentionnées précédemment et dans les mêmes conditions.

Mots clés

Goupille de poussée et insert, Tribomètre, la résistance à l'usure.

Abstract

Wear resistance is a critical factor in industrial applications, particularly in the oil and gas industry, where it can significantly impact maintenance costs and operational efficiency. This study focuses on the wear resistance analysis of thrust pin and insert in high-speed drilling motors. The first stage is to characterize them through different techniques which could identify their steel grade to be AISI 9314 steel for the thrust pin and AISI 9310 steel for the thrust insert. The second stage involves investigating their wear mechanisms using a tribometer tester then evaluating their wear behavior using profilometer and SEM integrated with EDS. The last stage is to enhance the thrust pin and insert performance through substituting AISI 9310 steels by AISI 4337 steel after testing the wear resistance using the same techniques mentioned before in the same conditions.

Keywords

Thrust pin and insert, Tribometer, wear resistance.

Dedication

To my precious family, especially my parents, I extend my deepest appreciation for their unwavering support throughout all of my studies. Their sacrifices and continuous encouragement have been the pillars of my success. To my two brothers, Yacine and Abdessamed, your presence in my life has brought colors and joy. Without you, my life would be devoid of the vibrant hues that paint my world.

To my dear uncle, thank you for your supportive words and unwavering belief in my abilities. Your guidance has been invaluable in shaping my path.

To my aunt, your support has been a constant source of strength. I am grateful for your presence in my life.

To my friends Meriem, Rania, Asma, Amani, and Wissal, thank you for the cherished memories we have shared. You have been and will always remain my sisters. Your friendship has brought laughter, joy, and unwavering support.

To my esteemed professor of chemistry at ESSA, the one and only Madam Dr. Zaioua Karima, I am indebted to you for your support, guidance, and valuable advice. Your expertise and dedication have shaped my understanding and passion for chemistry.

To the best physics professor in the world, Mr. Maghlaoui Nadir, I express my deepest appreciation. Your teachings have ignited my curiosity and love for the subject.

To all those mentioned and to those who have supported me silently along the way, I offer my heartfelt gratitude. This work is a culmination of our collective efforts and belief in the pursuit of knowledge.

10 July, 2023
National Polytechnic School
Sarra BERTAL

Dedication

Because "The beautiful thing about learning is that nobody can take it away from you." To my beloved mother, who enlightens my path of learning, this work is dedicated to you. In fact, it's your graduation and your success. Your encouragement, and sacrifices have shaped the person I am today. To Ibtissem the wisest sister ever, my soulmate and my first destination whenever I needed something. To the two troublemakers Alaa and Anes, without them my life would be boring. To my prettiest little sister Assoula, the indulged family member. Last but not least, to my aunt and cousins to whom I am and will be forever gratful for their support. To Bnat Flona, with whom I've shared my best moments at high school, because If you were not a mathematician, don't bother yourself talking to us. I'm truly chancy by having you in my life.

To Beyonders, and endless preparations of lesson plans and ice breakers, to Nesrine, Mustapha, Ahmed, Chirine, Habib, and Malik. To the big family of World Learning, with whom I started gaining valuable opportunities and leaving an impact on my society, to Habib and his unwavering support bearing all my questions, to Madam Aziza and Madam Leah, the most powerful women managers I've ever encoutered.

To my partner in crime Sarra, our shared moment in Elbaguel and Ghardia with the one and Only, Khali Mohamed would forever be stuck in my mind, yet I believe good and exciting days are to come. To all friends whom I enjoyed their company and joyful moments, this work is dedicated to you.

10 July, 2023
National Polytechnic School
Achouak Benarbia

Acknowledgment

First and foremost, we would like to express our deepest gratitude to God for providing us with the strength, wisdom, and guidance throughout our journey in completing this thesis. We would like to extend our heartfelt appreciation to Mr. ABADLI Kamel, our esteemed professor, for his unwavering support, invaluable guidance, and profound knowledge. Your expertise and dedication have played a pivotal role in shaping the direction and quality of this thesis. Your mentorship has been truly instrumental in our academic growth. We're immensely grateful to Miss. Asma Chekroune, the NAF recruiting manager at Schlumberger, and Mr. Hamada Fahmy, NAF WEC TLM manager for granting us the opportunity to conduct this project in collaboration with such a renowned organization. Your trust and belief in our abilities have been instrumental in making this project a reality.

Our deep gratitude is expressed to the esteemed members of our jury, Mr. DAIMELLAH Abderrahmane and Mr. SEDJAL Hamid for accepting to read and evaluate our final thesis. We would also like to express our sincere appreciation to : Mr. Abdelhak Bouderba Head of production department in BCR, and Miss. Amina Mechouat HR department in ENGTP, to Mr. Gana Mohammed Amin ex-Head of the corrosion department in CRD-SONATRACH for their remarkable services. To Mr. Hakim Mezoued, Co-head and technical responsible of ATP Mesrouk, and to Mr. Hacen Belalem, Technical department responsible at ATP Mesrouk for their support. To Mr. Amr Mahran, Operations manager at Arab Metals for his assistance. last but not least to Mr. Kherrouba Nabil, Former Researcher at CRTI for his patience and well receiving us at CRTI.

Without forgetting our teachers from the Department of Materials Engineering, to whom we will be eternally grateful for the efforts they have made throughout our academic path. In the memory of Mr. BOUABDALLAH Mabrouk, your sudden departure has left an indescribable void in our hearts and in the realm of Materials Engineering Department. May you rest in eternal peace.

Contents

List of Figures

List of Tables

List Of abbreviations

- AISI: American Institute for Steel and Iron.
- ASTM: American Society for Testing and Materials.
- ATP: Adjustage Tournage de Précision.
- BCR: Boulonnerie Clouterai Robinnerai.
- BEI: Backscattered Electron Imaging.
- BHA: Bottom Hole Assembly.
- CRTI: Centre de Recherche de Technologie Industrielle.
- D&I: Direction and Inclination.
- EDS: Energy-Dispersive X-ray Spectroscopy.
- ETD: Everhart Thornley Detector.
- E&P: Exploration and Production.
- GHI: Grit Hot-Pressed Insert.
- HSE: Health, Safety, and the Environment.
- HSLA: High-Strength Low-Alloy.
- MWD: Measurement While Drilling.
- OES: Optical Emission Spectroscopy.
- POOH: Pull Out Hole.
- ROP: Rate of Penetration.
- RPM: Rotations per Minute.

- SCC: Stress Corrosion Cracking.
- SEM: Scanning Electron Microscopy.
- SE: Secondary Electron.
- SEI: Secondary Electron Imaging.
- SPEC: SlimPulse Electronic Cartridge.
- SPBA: SlimPulse Battery.
- SPMA: SlimPulse Modulator Assembly.
- TSP: Thermally Stable Diamond Inserts.
- WOB: Weight on Bit.

List of symbols

- dP: Difference in pressure
- A3: Critical temperature of austenite transformation.
- HRc: Rockwell hardness type C
- HV: Vickers hardness.
- Ga: Grain size of the austenite.
- F: Frictional force
- F_N : Normal force
- f: Coefficient of friction
- τ: Shear strength
- H: Hardness
- W: Volume worn
- K: constant related to the probability of surface contact and debris formation.
- s: sliding distance
- P: the applied load
- P_m: Flow pressure

General introduction

Wear resistance is a critical factor in the selection of materials for industrial applications, particularly in the oil and gas industry. The wear-related challenges faced in this sector can have significant economic and technical implications, ranging from increased maintenance costs to compromised operational efficiency. To address these concerns, materials engineers play a pivotal role in selecting the most suitable materials for specific applications, with the objective of increasing the life cycle and optimizing performance. High-speed drilling motors used in the oil and gas industry operate under extreme conditions, subjecting critical components such as thrust pins and inserts to immense mechanical stress and wear. These components are vital for transmitting axial loads and withstanding the abrasive forces encountered during drilling operations. This thesis focuses on the comprehensive characterization and wear resistance analysis of thrust pins and inserts in high-speed drilling motors. Our primary objective is to investigate the wear mechanisms and evaluate the influence of steel grade substitution on the performance of these components. By replacing the existing materials with alternative steel alloys exhibiting superior wear resistance properties, we aim to optimize the functionality and increase the service life of thrust pins and inserts. Ultimately, this research aims to bridge the gap between theoretical knowledge and practical application, equipping materials engineers with the necessary insights to optimize the wear performance of thrust pins and inserts in high-speed drilling motors. The research consists of five chapters that explore various aspects of the topic. In Chapter 1, we provide an introduction and an overview of drilling operations, emphasizing the importance of thrust pins and inserts in high-speed drilling motors. Chapter 2 delves into metallography and heat treatments of structural steel, providing an understanding of the microstructural properties and heat treatment processes relevant to our study. Chapter 3 focuses on the wear behavior of steels, examining different wear mechanisms and factors influencing wear performance. We review relevant literature and research findings to gain insights into the wear characteristics of steel alloys. Chapter 4 outlines the experimental procedures followed in our research, including samples characterizing, wear testing, and material selection. In the final chapter, Chapter 5, we present the results obtained from the wear testing experiments and provide a detailed interpretation of the data. We analyze the wear characteristics of different steel grades, evaluate their performance, and assess the effectiveness of steel grade substitution in enhancing wear resistance. The thesis concludes with a summary of the findings and their implications for optimizing thrust pins and inserts in high-speed drilling motors. We also provide perspectives for future research directions and potential avenues for further improving wear resistance in drilling components.

First part

Bibliographic study

Chapter 1

Overview on drilling operations

1.1 Introduction

Crude oil has significant value as one of the most prized energy resources. Serving as a fundamental component of petroleum, it powers vehicles, ships and planes. Moreover, it serves as an essential raw material in a range of products, including petrochemicals, lubricants, plastics and synthetic materials. The oil and gas industry is divided into three segments: upstream, midstream and downstream.

- **Upstream**, also known as exploration and production (E&P), deals with locating reservoirs and drilling wells to extract oil and gas.
- **Midstream companies**, operating in the intermediate stage, assume the responsibility of transporting resources extracted from wells to refineries.
- **Downstream companies** are responsible for refining and marketing of finished products.

The process of extracting, refining, and utilizing crude oil requires significant labor input, potentially involving numerous individuals ranging from hundreds to even thousands. The oil drilling industry and its related products contribute to employment opportunities across various sectors. Job creation and subsequent economic growth are immediate advantages associated with oil drilling [1,2].

1.2 Oil and gas well drilling

Drilling in the oil and gas industry involves the use of a mechanical rig designed to penetrate the earth's subsoil by creating a hole. The main purpose of drilling is to perform various well-related tasks such as acquisition, development, storage, injection and production of oil and gas [3]. Drilling a well encompasses the preparation of diverse parameters, equipment, and tools essential for the physical drilling procedure. A notable example is the utilization of torque and drag software during well planning, which facilitates the identification of suitable drill pipes capable of withstanding the encountered torque and drag forces [4].

1.2.1 Types of platforms and equipment

There are different types of drilling rigs, each designed to meet specific drilling conditions and operational needs. Land rigs are mainly used for onshore drilling, while offshore rigs

are employed in drilling operations conducted in oceans or other bodies of water. Offshore platforms can be categorized into jack-up rigs, semi-submersible rigs, and drillships (as shown in Figure 1.1), each offering unique capabilities for drilling in different water depths.

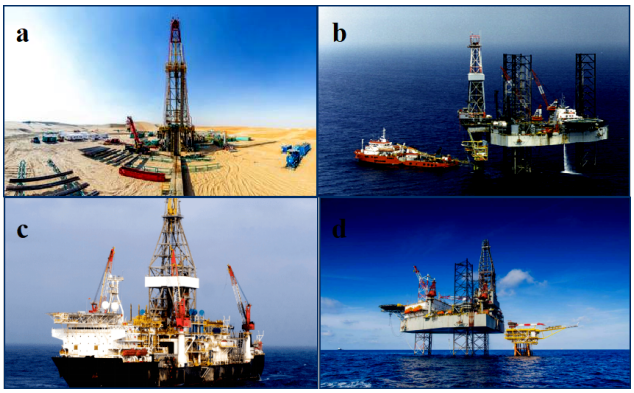

Figure 1.1: Types of rigs include: a/ land rig, b/ jack-up rig, c/ drillship, d/ semi-submersible rig [5, 6, 7, 8].

In Algeria, the only type of machine available is the land machine which requires regular assembly and disassembly for transport between different sites. These land rigs must possess certain characteristics: rapid ascent and descent, independence from specialized cranes for erection, sufficient power to lift the drill pipe and casing to the required depth, and maximum power availability. for circulation of the drilling fluid [9]. The platform includes virtually everything except the living quarters. Major components include blowout preventer, mud tanks and mud pumps, derrick or mast, traction devices, rotary table, Kelly or top drive, drill string, drill bit, l power generation equipment and auxiliary equipment [10].

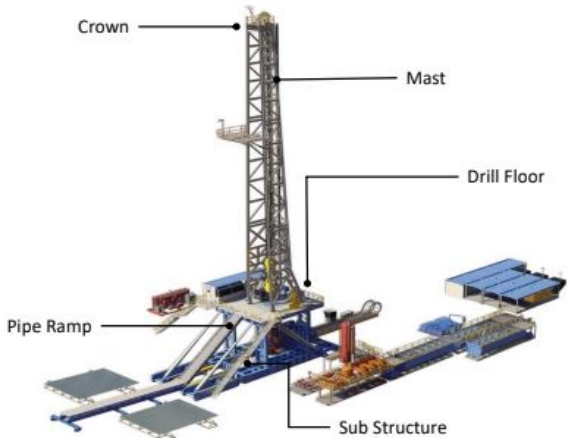

Figure 1.2: Land platform structures [11].

1.2.2 Drilling process

1.2.2.1 Planning

Well planning is a very difficult aspect of drilling engineering, requiring the integration of engineering principles, individual or corporate considerations, and past experience. Although well planning methods may change from industry to industry, the ultimate goal is to successfully drill a well that meets the reservoir engineer's production requirements while ensuring safety and minimizing cost [12].

1.2.2.2 Drilling

The drilling process begins with leveling and preparing the ground. A drill bit, attached to a drill string and powered by a motor, is used to create a borehole in the ground. Drilling depths can range from 1200 m to 3500 m for oil reserves, with diameters varying from 12 centimeters to one meter. The borehole is formed by gradually drilling smaller sections, starting with the largest diameter at ground level [13]. During the drilling process, the length of each section is determined by evaluating the formation pressure at the bottom and comparing it to the fracture pressure at the top. This assessment ensures the proper section length for safe and efficient drilling. After drilling each section, a steel casing is inserted into the well and secured with cement. Casing serves several purposes, including isolating different formations, protecting freshwater aquifers, providing structural integrity, and strengthening the well as drilling progresses to greater depths. Throughout the drilling process, drilling mud circulates to cool and lubricate the drill bit, support the borehole, prevent the influx of formation fluids, remove the drilled cuttings and transport them to the surface [10].

1.2.2.3 Completion

When the drilling and casing process is complete, the next step is to complete the well to allow for proper use. Eventually, the drill crew reaches the bottom of the well, often indicated by encountering a reservoir rock composed of sand or clay. The drill is then extracted from the ground and tests are carried out to confirm the success of the well [9,13].

1.2.2.4 Production

After creating perforations in the casing to allow the movement of oil, a tube is inserted and surrounded by a protective casing using a packing device. A Christmas tree is installed on top, controlling the flow of oil and access to the wellbore. Safety measures such as pressure gauges and shut-off valves can be added. The system optimizes oil production while ensuring control and safety. Once the oil is flowing, the rig is removed and a pump attached to the well opening propels the oil upwards using an electric motor and a lever mechanism [13].

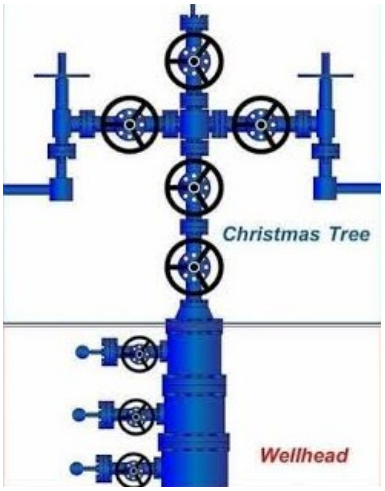

Figure 1.3: Christmas tree [14].

1.3 Safety and environmental considerations

In the highly competitive drilling industry, health, safety and the environment (HSE) are the first consideration in any drilling program. The primary objective of any security audit is to systematically and critically assess all potential hazards involving personnel, platform, services and operational methods to ensure that existing health and safety practices fully meet the requirements stipulated by law [15].

1.4 Drilling technology and equipment used

1.4.1 SlimPulse: MWD tool

The MWD measurement tool stands for Measurement While Drilling, allows to provide measurements that help us to determine the orientation of the drill bit which allows us to

determine the position of the borehole and to steer the well. These measurements are actually taken during the drilling of the well. The most common MWD tool, which was used and requested by the customer in this case study, is called SlimPulse. The recoverable SlimPulse is the third generation slim MWD service, it gives real-time direction, tilt, tool face and gamma ray measurements for mud pulse telemetry. It relies on measurements of the Earth's magnetic and gravitational fields to determine the orientation of the downhole assembly, while continuous direction and inclination (D&I) measurements are made during rotation to aid in trajectory control and reduce stationary measurements. SlimPulse Chain basically consists of three main assemblies: SlimPulse Modulator Assembly (SPMA), SlimPulse Battery (SPBA), and SlimPulse electronic cartridge (SPEC). The SPMA is the mechanical part of the SlimPulse that serves as the tool data telemetry and power generator for the rest of the components, while the battery SPBA, powers the entire SlimPulse tool. It is a through-hole battery assembly that can be connected above or below the SPEC.

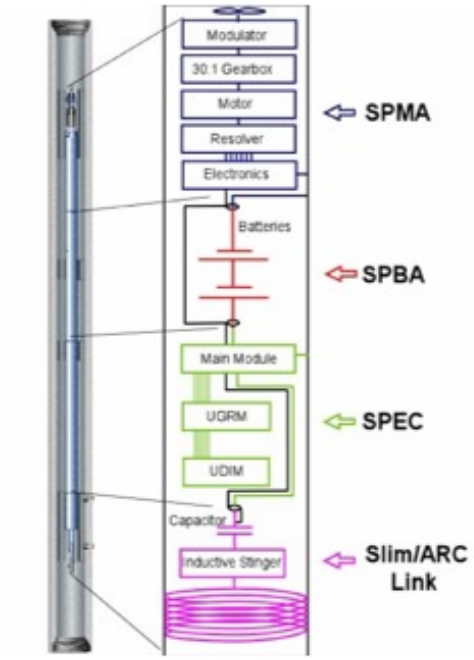

Figure 1.4: Different parts of SlimPulse [16].

1.5 High speed motor

A drill motor, also known as a mud motor, is a pump used in drill strings to enhance the power of drill bits. By utilizing drilling fluid or mud, the motor creates eccentric motion in its power section. This movement is then transmitted to the concentric power, ultimately driving the drill bits. To optimize performance, drill motors employ various rotor and stator configurations, with increased lobes and power section length resulting in higher power output. Drill motors are primarily employed in directional drilling, which consists of two modes: sliding (construction) and rotary (straight drilling). In sliding mode, the drill string remains stationary at the surface, and the adjustable curvature of the drill motor is steered in the desired drilling direction. On the other hand, in rotary mode, the drill string rotates, and the motor curvature does not affect the drilling direction, resulting in straight drilling. Motors play a crucial role in drilling operations involving complex well trajectories, often operating under aggressive settings in harsh environments to improve drilling efficiency. However, it is not uncommon for drilling activities to encounter inefficiencies and delays that deviate from the initial plans. Schlumberger (Slb), with its extensive experience, has managed to control these aggressive parameters with high-performance motors. Nonetheless, they still face challenges in countries like Algeria, where the demanding and aggressive formation necessitates the use of a special type of motor called high-speed (HS) motors. Despite this, these motors are susceptible to damage caused by these parameters. Slb collaborates with Radius-services, a Russian company that provides various services, including HS mud motors. These motors are predominantly used in difficult or challenging geological formations encountered in Algeria. This thesis aims to investigate a specific challenging case that causes severe engine damage, leading the engineers to pull out of hole (POOH) the bottom hole assembly (BHA) after several attempts to resolve the problem. To begin, we will provide an overview of the different components of this high-speed engine.

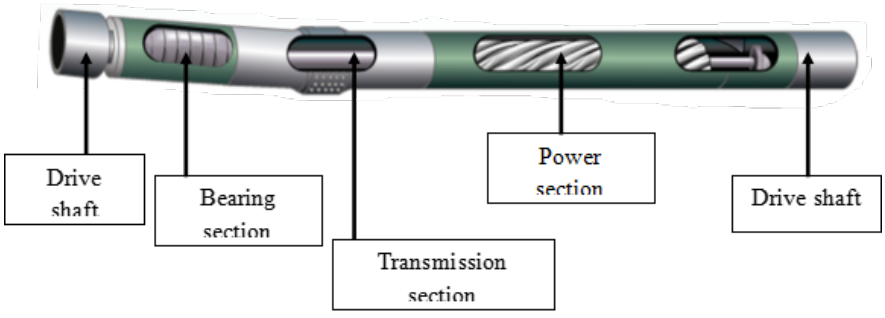

Figure 1.5: Diagram of mud motor with different parts [17].

1.5.1 Description of the different parts of the HS motors

1.5.1.1 Power section

The power section of a mud motor consists of a rotor and a stator, which work together to convert hydraulic energy from the mud into mechanical power. This mechanical power is utilized to rotate the drill bit during drilling operations. To achieve this, mud is pumped into the power section at high pressure, causing the rotor to rotate within the stator. The resulting rotational force is then transmitted to the drill bit through a transmission shaft and a drive shaft. The rotor is typically made of stainless steel to prevent corrosion, and it is often coated with a thin layer of chrome plating to minimize friction and wear. On the other hand, the stator is a steel tube that contains a rubber liner molded into its bore. The rubber liner is specifically designed to withstand abrasion and degradation caused by exposure to hydrocarbons. Both the rotor and the stator have helical profiles, but they differ in the number of spirals or lobes. The rotor typically has one less lobe compared to the stator. In the case of high-speed motors, the power sections are configured with a 2:3 lobe arrangement, resulting in a higher rotational speed and, consequently, a greater power output.

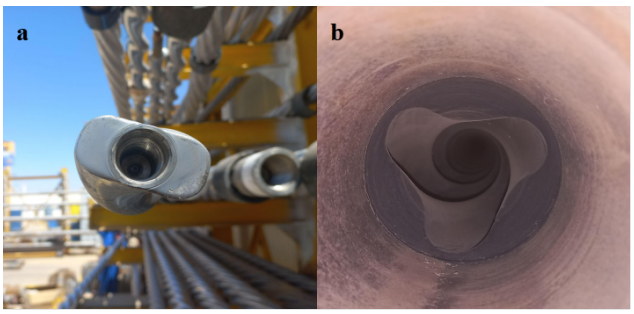

Figure 1.6: Power section of a high-speed motor representing a) the rotor and b) the stator.

The rotor and stator of the mud motor are sealed where they make contact, forming multiple separate cavities arranged in a straight line. As mud is pushed through these cavities, it induces a rotational movement in the rotor within the stator, known as nutation. For each cycle of nutation completed inside the stator, the rotor rotates by the width of one lobe. Therefore, the rotor needs to undergo nutation for each lobe of the stator in order to complete one revolution of the bit box. The length of each stage is determined by the angle of inclination of the spiral lobes. When the pitch angle increases, the stage length becomes shorter, resulting in tighter turns and a decrease in the vector force perpendicular to the rotor's longitudinal axis (torque) as well as a reduction in the volume of the cavity inside the rotor while the motor speed increases. In the specific case study mentioned, the high-speed motor follows a 2:3 lobe configuration with a stage length of 8.5 feet.

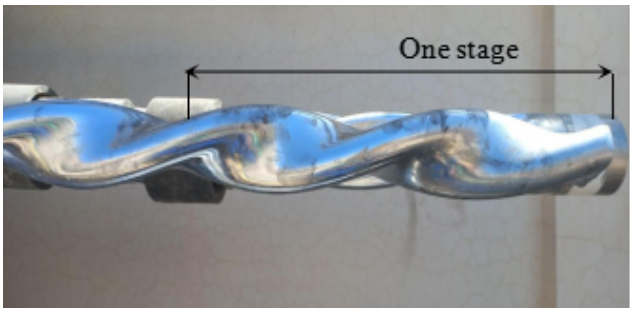

Figure 1.7: Spiral stage length of rotor.

1.5.1.2 Transmission section

In the transmission section of the mud motor, its primary function is to convert the eccentric motion of the rotors into concentric motion at the bearing and drive shaft. Additionally, it serves to compensate for the rotor's nutation eccentric movement and absorb the downward thrust generated. The rotor is connected to the transmission section through a rotor coupling. This rotor coupling is linked to a cylindrical bar known as the transmission shaft. The transmission shaft plays a crucial role in transforming the eccentric motion into concentric motion. It is further connected to the bearing through a shaft coupling, ensuring a smooth and efficient transfer of power.

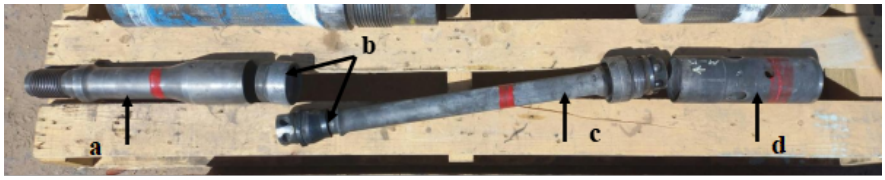

Figure 1.8: Transmission section parts representing a) Rotor coupling b) seals c) Transmission shaft d) Shaft coupling.

1.5.1.3 Thrust pin and insert

At each end of the transmission shaft, there are metallic components that facilitate the connection between the shaft and the coupling (rotor coupling and shaft coupling). One of these components is the thrust pin, a cylindrical pin typically made of hardened steel. Its placement within the transmission shaft enables it to transmit axial or thrust loads along the shaft. These loads can arise from factors like weight on bit (WOB), torque, or drilling forces. The thrust pin plays a vital role in distributing and supporting these axial loads, thereby ensuring the efficient and smooth functioning of the mud motor. The other component is the thrust insert, designed to interface with the thrust pin. The insert is usually made of

a low-friction material or other self-lubricating materials. It is positioned within rotor and shaft coupling and provides a smooth surface against which the thrust pin can slide. By reducing friction and wear between the pin and the shaft, the insert enables the efficient transfer of axial loads.

Figure 1.9: a) thrust pin, b) thrust insert.

The combined action of the thrust pin and insert is crucial for maintaining the integrity of the transmission shaft under high axial loads. Their presence helps prevent excessive wear and minimize energy loss caused by friction. By enhancing durability and performance, they contribute to smooth drilling operations, particularly in challenging drilling environments. The transmission shaft is designed to withstand the considerable forces and shocks generated by the rotor, which are expected to cause significant damage. However, to protect the transmission shaft from severe damage, both the rotor coupling and the shaft coupling are connected to the transmission shaft through the Thrust Pin and Insert. The purpose of these two components is to act as a sacrificial element that absorbs shocks and potential damage instead of the transmission shaft. While they're designed to endure and bear damage for a certain period, there are instances where they fail to function as efficiently as intended due to high-intensity forces and shocks. When the thrust pin gets damaged, it can develop a protrusion or deformation. As a result, when the damaged pin comes into contact with the insert, it creates impact marks on the thrust insert. The continuous shocks and impacts can lead to the formation of visible indentations or prints on the insert's surface. These failures can lead to significant issues, prompting engineers to perform a Pull Out of the Hole (POOH) operation on the Bottom Hole Assembly (BHA) where they need to replace the trust pin and insert to restore the proper functioning of the mud motor. Studying, analyzing and solving this problem will be the objective of this thesis.

Figure 1.10: New thrust pin and insert compared to damaged ones.

In the assembly's transmission section, there is a provision for an adjustable elbow box that can be controlled from the drill floor. The standard adjustable bent housings in this section offer the flexibility to accommodate bends ranging from 0 to 3 degrees, while certain motors may have 0 to 2 degrees adjustable housings. In the case of short radius motors, a 0 to 4 degrees adjustable housing is available. This range of adjustable housings allows for the customization of the drilling trajectory according to specific operational requirements.

Figure 1.11: Surface adjustable bent housing.

1.5.1.4 Bearing section and drive shaft

The bearing section plays a crucial role in supporting and transmitting loads, torque and speed from the driveshaft to the bit. It includes a sturdy drive shaft, usually made of forged steel, which is held in place by axial and radial bearings. Depending on the drilling needs, the bearing housing can have a smooth surface or be equipped with a sleeve that can be replaced on the drilling floor or an integrated stabilizer with blade-like extensions. These stabilizers are available in different diameters to suit different applications. To ensure proper lubrication and prevent damage to bearing components, two options are available: mud lubrication or oil sealing. In the first case, drilling mud is circulated through the bearing section to minimize friction and cool the components, while in the second case, a sealed lubrication system is used to isolate the bearings from the drilling environment [18].

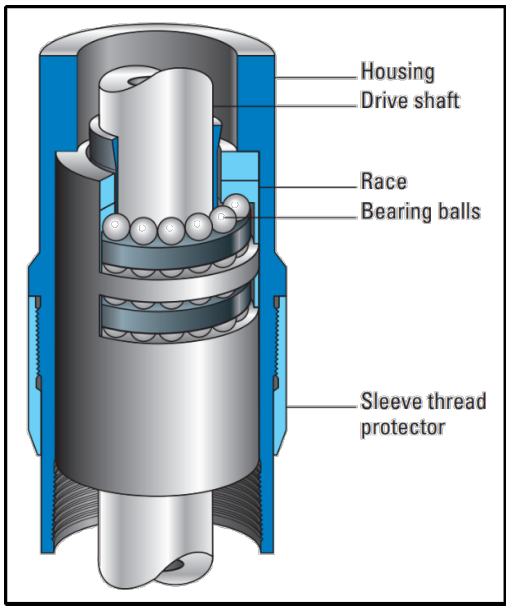

Figure 1.12: Diagram of the bearing section [18].

1.6 Drill bits

Drill bits are specialized cutting tools used in drilling boreholes for oil and gas exploration, production and extraction. These drill bits are designed to withstand the extreme conditions of drilling through various rock formations and geological formations encountered during the drilling process. The choice of bit depends on the type of formation to be drilled, drilling parameters such as weight on bit (WOB) and rotational speed, and the economics of the drilling operation.

Figure 1.13: Smith drilling bits.

1.6.1 K505 Impregnated Diamond Bit.

Kinetic Impregnated Diamond Drill Bits are engineered for superior performance when drilling at high RPMs in the hardest and most abrasive formations. The diamond crystals are embedded in the rib of the tungsten carbide matrix as shown in (Figure 1.14). This tool acts like a grinding wheel. The matrix binder wears out faster than the diamond, when the diamond eventually wears out it falls off and new diamonds are exposed as the binder wears out.

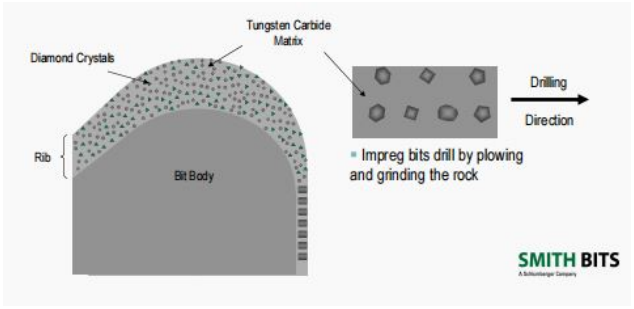

Figure 1.14: K505 impregnated diamond bit.

Important features

- Thermally stable diamond inserts (TSP) are placed on the gauge to maximize gauge retention and extend bit life.
- Turbine sleeves reduce vibration and hole spiraling in turbine applications. This feature increases bit life and enables the bit to achieve maximum ROP.
- Superior GHI (Grit Hot-Pressed Insert) diamond distribution increases durability and ensures maximum ROP for longer periods of time.

- Open bit face improves hydraulic flow and optimizes cleaning for increased ROP.

1.6.1.1 Drilling parameters

Drilling parameters are the variables that control a drilling activity. These parameters can be broadly classified into two types: Rig and Bit Related Parameters that can controlled, and Formation Parameters that have to be dealt with. Some of the drilling parameters that control a drilling activity include: WOB, RPM, pumping hours, Depth, (ROP), and Drilling fluid properties.

Table 1.1: Drilling parameters.

Parameter	**Temperature (°C)**	**RPM**	**ROP (m/h)**	**WOB (tonne)**	**dP (psi)**	**Flow rate (GPM)**	**Mud weight (Kg/m3)**
Value	101	30	0.82	0.5-18	100	51	1340

Chapter 2

Metallography and heat treatments of structural steels

2.1 Introduction

Structural steel refers to a specific grade of steel that is designed and manufactured for use in construction projects where load bearing capacity and structural integrity are critical. It is designed to provide strength, durability and stability to various types of structures. Its versatility makes it a preferred choice for engineers and architects when designing and constructing safe and efficient structures such as buildings, roads, bridges and other infrastructure projects requiring high weather resistance. Structural steels are classified in two ways:

- According to the chemical composition.
- According to use.

2.2 Classification of structural steels

2.2.1 Classification according to chemical composition

The chemical elements that enter into the constitution of structural steels are of two types:

- Production elements (carbon, silicon, manganese, sulfur and phosphorus).
- Elements of addition (silicon, manganese, chromium, nickel, molybdenum, vanadium, aluminum).

The classes of structural steels according to the chemical composition are:

2.2.1.1 Unalloyed steels

These steels contain the elements of elaboration (C, Si, Mn, S, P) in their composition and are distinguished by the carbon content.

2.2.1.2 Low alloy steels

Low alloy steels contain additional elements, including those found in unalloyed steels, as well as specifically selected and added elements at defined and studied rates. This deliberate combination enables the attainment of desired properties. The class of low alloy structural steels is categorized based on the specific groups of elements that are added to:

- Silicon alloy steels.
- Steels alloyed with manganese.
- Chromium alloy steels.
- Nickel alloy steels.
- Steels alloyed with chromium – manganese.
- Steels alloyed with chromium – molybdenum.
- Steels alloyed with chromium – vanadium.
- Steels alloyed with chromium – nickel or with nickel – chromium.
- Steels alloyed with nickel-chromium-molybdenum.
- Steels alloyed with chromium – nickel – molybdenum.

2.2.2 Classification according to use

Structural steels find application in various industrial sectors such as the mechanical industry, metallurgy, electricity, metal construction, rail transport, aeronautics industry, shipbuilding industry, and the hydrocarbon industry, among others. Each sector demands specific properties, necessitating the use of defined classes of steels. The classification of structural steels encompasses distinct steel groups tailored to meet the requirements of these sectors as follow:

- General purpose steels.
- Steels for heat treatments in the mass.
- Steels for carburizing.
- Steels for nitriding and carbonitriding.
- Steels for pressure vessels.
- High elastic limit steels.
- Spring steels.
- Bearing steels.
- Steels for bar turning.

2.3 Influence of alloying elements

In these steels, the rates of elaboration elements are limited by the standards and the rate of each addition element must not exceed 5%. Chemical elements present in the steel have an influence on the structure and on the properties.

- **Carbon (C)** Carbon plays a crucial role in steel, as it contributes to the hardening of iron and significantly enhances toughness and strength through solid solution effects in ferrite and austenite, as well as precipitation of cementite and martensite. A higher carbon content yields a material with greater strength but reduced ductility. In the case of most structural steels, the carbon content typically falls within the range of 0.15 to 0.35%. Exceeding this range results in diminished ductility, while falling below 0.15% compromises the desired strength levels.

- **Silicon (Si)** Along with aluminum, silicon is one of the main de-oxidizers in structural steel. It appears in amounts below 0.40%. Silicon, an alpha-gen element, strengthens ferrite.

- **Manganese (Mn)** The presence of manganese in structural steel grades generally ranges from about 0.50% to 1.70%. It exhibits effects similar to carbon and is often used by steel producers in conjunction with carbon to achieve the desired mechanical properties by solid solution effect and by its pearlitizing effect. Manganese contributes to lowering the sulfur rate through the formation of the MnS compound which is eliminated during production.

- **Phosphorus (P) and sulfur (S)** Both of these are generally undesirable due to their negative effects on the material. Sulfur, in particular, contributes to internal segregation in the steel matrix, while sulfur and phosphorus can reduce the ductility of the material. Therefore, steel grade specifications impose strict limits on the allowable amounts of phosphorus and sulfur, generally limiting them to levels below about 0.04% to 0.05%.

- **Chromium (Cr)** Chromium, an alpha-genic and carbide-forming element, improves resistance, hardenability, resistance to abrasion and resistance to atmospheric corrosion. However, this decreases the weldability. In the case of low alloy steels with minimal chromium content, they have a higher creep resistance than carbon steels, which makes them suitable for applications requiring increased strength at high temperatures.

- **Nickel (Ni)** Nickel, a gamma-genic and non-carbide-forming element, not only contributes to the corrosion resistance of steel, but also improves its performance in low

temperature environments by improving fracture toughness. It also increases ductility and fracture transition temperature, but it can cause aging.

- **Molybdenum (Mo)** Molybdenum, an alpha-genic and carbide-forming element, shares similarities with manganese and vanadium in terms of effects, and is frequently combined with one or the other. Its inclusion notably improves the steel's resistance to high temperatures while also improving corrosion resistance. For specific grades of A588 steel, typical amounts of molybdenum range from 0.08% to 0.25%, while various types of A514 may contain molybdenum in the range of 0.15% to 0.65%.

- **Vanadium (V)** Vanadium, an alpha-genic and carbide-forming element, having the same effect as Mn, Mo and Cb, it helps the material to develop a finer crystalline microstructure and gives increased resistance to fracture. Vanadium contents of 0.02% to 0.15% are used in ASTM grades A572 and A588, and amounts of 0.03% to 0.08% in A514 [1].

- **Aluminum (Al)** Aluminum is of significant importance as a deoxidizer in steel, contributing to the formation of a finer crystalline microstructure. It is commonly used in conjunction with silicon to achieve a semi or fully killed steel composition.

- **Copper (Cu)** Another essential element for corrosion resistance is present in steel grades, usually in amounts not less than 0.20%. It serves as the main component to combat corrosion in steel grades such as A242 and A441.

2.4 Heat treatments of structural steels

Structural steel can encounter various challenges when in service, most structures are exposed to high humidity environments, they can also be subjected to overloads or cyclic loading, leading to cracking and eventual failure. The structural steel must withstand these conditions and show better performance. One of the essential practices used to mitigate these hazards is heat treatment. Heat treatment is a widely used process in the steel industry that involves controlled heating and cooling of steel which can alter its microstructure and provide a wide range of mechanical properties. On the other hand, the addition of alloying elements also plays a significant role in influencing the response of steel to heat treatment. It generally comprises three stages: austenitization, quenching and tempering.

2.4.1 Austenitization

Austenitizing is a heat treatment process involving heating and holding the material at an austenitizing temperature of A3 + 50°C. It facilitates the final redistribution of alloying elements between the austenitic matrix and the retained carbides. This redistribution determines the chemical composition, volume fraction, and dispersion of the retained carbides. These alloy carbides play a dual role by contributing to wear resistance and influencing the austenitic grain size. Finer carbides and a higher volume fraction of carbides effectively control the growth of austenitic grains. However, excessive austenitizing temperatures pose the risk of undesired grain growth as the alloy carbides may grow larger or dissolve into the austenite. During the austenitizing process, continuous monitoring and control of the internal furnace environment are crucial to prevent carburization or decarburization of the parts. In the case of vacuum furnaces, it is essential to maintain low leakage rates and regulate the partial pressure at austenitization temperatures, particularly when they exceed 1095°C [2].

2.4.2 Hardening

The cooling process from the austenitizing temperature depends on the composition and thickness of the part. Cooling options include water, brine, oil, salt, inert gas or air. Slow cooling in the furnace is called annealing. However, annealing is not commonly used except as an intermediate treatment to facilitate the machining of certain grades. On the other hand, cooling the part in still air is known as normalizing, which is the most commonly used treatment and provides good strength and ductility. Rapid cooling in water or oil is known as quenching. In the case of air quenching, the transformation of austenite does not occur at a specific constant temperature. Instead, this transformation takes place over a range of temperatures, which can lead, for example, to the formation of martensite and bainite, or a combination of pearlite, bainite and martensite. The quenching medium selected should cool the part at a rate that achieves the desired hardness. It is important to avoid using a quenching medium with excessive cooling capacity beyond requirements, as this may lead to cracking or excessive distortion. Careful consideration of the quenching process is necessary to strike a balance between achieving the desired hardness and preventing adverse effects on the part [2, 3, 4].

2.4.3 Tempering

Tempering is a heat treatment process that can improve the ductility and toughness of martensite resulting from quenching. Tempering consists of heating the martensite to a

temperature between approximately 121and 249°C, maintaining it at this temperature for a short time, then cooling it slowly. This process enables the diffusion of excess carbon in the martensite, leading to the formation of small cementite particles within the ferrite matrix. The resulting tempered martensite has a fine microstructure with many cementite particles distributed throughout the ferrite matrix. These particles act as barriers to dislocation motion during plastic deformation, which improves the ductility and toughness of the material while maintaining its hardness and strength [5].

2.4.4 Hardenability

Hardenability is the property of steel that describes its ability to undergo deep quenching or hardening in a cylindrical bar of diameter D and cross section to form martensite and prevent the formation of ferrite, pearlite and bainite.

2.4.4.1 Factors influencing hardenability

Hardenability should not be confused with hardness, as hardness is a material property related to resistance to penetration and proportional to strength. It is crucial to understand that hardness is only influenced by the carbon content of the steel. On the other hand, hardenability refers to the ability to reach a specific hardness at a particular depth, and it is influenced by several factors. The actual depth of hardness depends on: the size and shape of the section, the presence and amount of alloying elements, and the austenitizing conditions [6].

- **Influence of alloying elements** All alloying elements, except cobalt, when dissolved in austenite have a favorable effect on hardenability, as they make austenite more stable and retard its transformation by nucleation and growth. Alloyed steels have better hardenability than less or unalloyed steels. Figure 2.1 compares the hardness of three steel grades as a function of added alloying elements [7]. On the other hand the influence of certain alloying elements on the hardenable diameter has been studied by R.A. Grange, and is illustrated in Figure 2.2. The hardenable diameter (ΔD) refers to the diameter of the cylinder which results in the formation of 90% martensite in its core after rapid cooling in water.

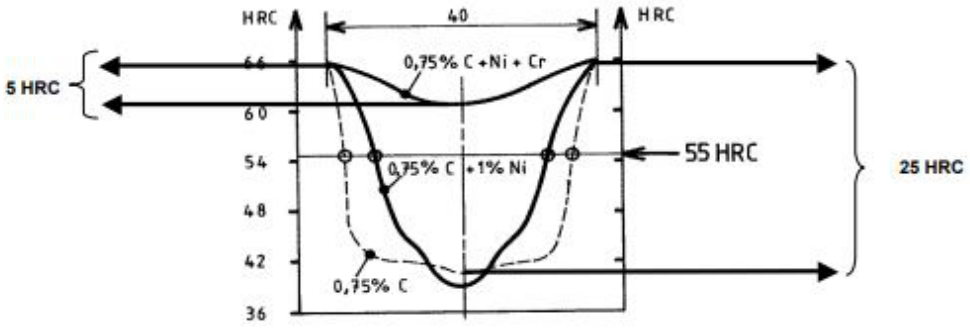

Figure 2.1: Hardenability curve showing the effect of adding Ni and Cr on the hardenability of 0.75% steel [8].

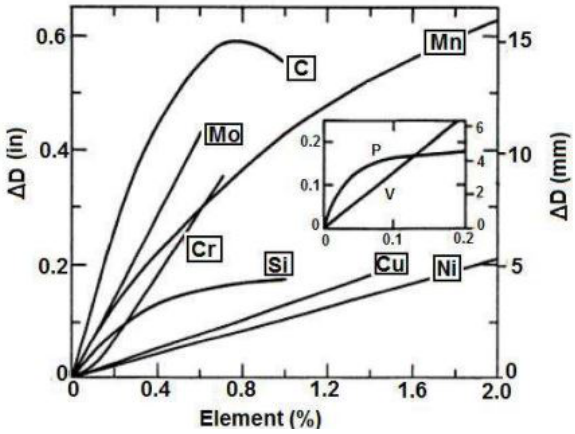

Figure 2.2: The change in the hardenable diameter (ΔD) due to composition variation in shallow-hardening steels [9].

- **Influence of austenitization conditions** The austenitizing conditions are determined by the austenitizing temperature and time (Ta and ta respectively). These two parameters have a direct effect on austenite homogeneity and austenitic grain size (called Ga index). The higher Ta and ta are, the more homogeneous the austenite becomes and the larger the grain size (lower Ga value), resulting in higher hardenability, as shown in Figure 2.3 [7].

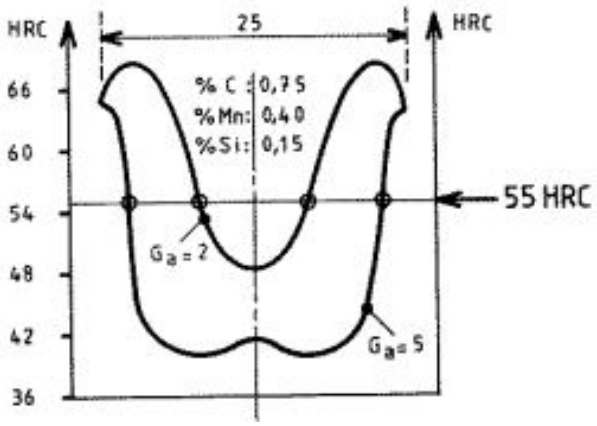

Figure 2.3: An increase in Ga improves hardenability but adversely affects mechanical properties [8].

2.5 Properties of steel

Structural steel offers an exceptional strength-to-weight ratio, allowing it to support heavy loads while remaining lightweight. This inherent property makes it well suited for the construction of expansive edifices such as bridges and skyscrapers, as well as smaller items including handrails, ladders and possibly push pins and inserts.

2.5.1 Mechanical properties

The mechanical characteristics of structural steel are remarkable. It has sufficient strength to support substantial loads, while offering the flexibility to be formed into various shapes without succumbing to fractures or cracks under pressure. In addition, structural steel has favorable fatigue resistance, which allows it to withstand cyclic loads without suffering permanent deformation or long-term damage. These qualities make it an ideal choice for applications such as car chassis and suspension systems, where these properties are crucial to ensure safe operation.

- **Tensile Strength**: Structural steel has a high tensile strength, which means it can withstand high loads before breaking. In general, the tensile strength ranges from 400 to 550 MPa [10].
- **Hardness**: This is an essential property of structural steel that determines its resistance to indentation, wear and deformation. Structural steel is often designed to possess a balanced level of hardness, striking a careful balance between strength and toughness. By carefully choosing the composition and heat treatment processes, the hardness of structural steel can be tailored to meet specific application requirements [12]. A

tempered steel alloyed with Cr and Ni can have a hardness value varying from 35 HRc to 41 HRc, depending on the carbon content and tempering temperature.

- **Ductility**: Structural steel exhibits excellent ductility, allowing it to be easily shaped, bent and shaped. The ductility of structural steel is usually expressed in terms of area elongation or reduction in a tensile test. Typically, structural steel grades have ductility values ranging from 15% to 30% elongation or more, depending on the specific grade and processing conditions. This high ductility ensures that the structural steel can withstand dynamic loads, absorb energy and maintain structural integrity [10].
- **Toughness**: is measured by the amount of energy required to break the material at a certain temperature. In other words, the ability to absorb energy and resist breaking under impact or sudden loads. It combines strength and ductility and is often measured using impact tests [10].
- **Fatigue Strength**: refers to the resistance of steel to failure under cyclic loading or repeated stress cycles. It measures the material's endurance and resistance to fatigue cracking. Fatigue resistance depends on strength, ductility, service conditions, corrosion, residual stresses in the component, design (especially in high stress areas), surface finish and the required lifetime of the component [10].
- **Stiffness**: Elastic stiffness is the measure of the steel's ability to support the loads applied to it without plastic deformation. It is influenced by several factors, including Young's modulus, chemical composition, and heat treatment [11].

2.5.2 Physical properties

- **Density**: One of the most important physical properties of structural steel is its density. Indeed, the thickness of the steel directly affects its strength. The higher the density of the steel, the stronger it will be. The density of steel can range from 7,850 to 8,050 Kg/m^3 [12].
- **Elasticity**: Young's Modulus is a key physical property of structural steel, indicating its elasticity and ability to return to its original shape after deformation. With a higher Young's modulus (ranging from 190 to 210 GPa), steel can withstand stresses without permanent deformation. Additionally, the yield strength of structural steel (ranging from 250 to 1500 MPa) measures its resistance to forces that can cause permanent deformation, highlighting its strength [12].
- **Magnetic properties**: The magnetic properties of steel mainly depend on the microstructure and the presence of ferromagnetic alloying elements. That is, adding

nickel, cobalt can increase the magnetism of steel, while non-magnetic alloy such as chromium and molybdenum can make it non-magnetic by stabilizing the austenitic structure which is essentially a non-magnetic crystal structure. On the other hand, the magnetism of steel increases with decreasing carbon content [13].

- **Thermal Conductivity**: The thermal conductivity of a material is a measure of its ability to conduct heat. The lower the thermal conductivity, the better the material will insulate against heat transfer. The thermal conductivity of structural steel can vary from 25 to 100 watts per meter Kelvin [12].

2.5.3 Weldability

The ability of a metal to undergo welding under given manufacturing conditions and form a structurally suitable design, while performing adequately during its lifetime. Weldability is influenced by a variety of factors, including the composition and treatment of the steel, as well as the properties of the weld metal and the heat-affected zone (HAZ). The choice of welding variables, such as heat input and welding technique, also plays an important role. Additionally, pre- and post-weld treatments, such as preheating, stress relieving, and heat treating, can impact the weldability of a metal. Consideration of these factors is essential to ensure successful welding operations and achieve the desired welding quality and performance [14].

2.5.3.1 Carbon equivalent

The carbon equivalent CE is used to predict the properties of steel. It helps determine properties such as hardenability and susceptibility to hydrogen cracking (cold cracking). The concept of carbon equivalence applies to ferrous materials and considers alloying elements in addition to carbon. CE indicates the probability of martensite formation during cooling and brittle failure. The carbon equivalent of steel is usually calculated using the additive rule accepted by the American Welding Society (AWS) in equation (2.1):

$$CE = C + \frac{P}{2} + \frac{Mn}{6} + \frac{Mo}{4} + \frac{Cr+V}{5} + Ni \tag{2.1}$$

CE c̄arbon equivalent, C c̄arbon, P p̄hosphorus, Mnm̄anganese, Mo m̄olybdenum, Cr c̄hromium, V v̄anadium and Ni n̄ickel. Lower carbon equivalent values indicate better weldability for the steel under consideration, while higher CE values suggest potential difficulties when welding. Table 2.1, shown below, illustrates the range of carbon equivalent values and their corresponding impact on weldability, including cases requiring preheating [15].

Table 2.1: Range of CE for weldability and preheating of steel [15].

Carbon equivalent CE	Weldability	Preheating
Up to 0.35	Excellent	Not necessary
0.36 0.40	Very good	Recommended
0.41 0.45	Good	Necessary
0.46 0.50	Fair	Necessary
0.51 and over	Poor	Necessary

2.6 Steels alloyed with nickel-chromium-molybdenum

Steels alloyed with nickel-chromium-molybdenum (Ni-Cr-Mo) are commonly used in various industries due to their excellent combination of mechanical properties, corrosion resistance, and wear resistance. These steels offer high strength, toughness, and resistance to both general and localized corrosion. An overview of the chemical composition ranges can be further seen in table 2.2 [16].

2.6.1 Chemical Composition Ranges

The chemical composition of Ni-Cr-Mo steels may vary, but typical ranges are as follows: Other elements such as copper (Cu), vanadium (V), and tungsten (W) may also be present

Table 2.2: Chemical Composition Ranges of Ni-Cr-Mo Steels [16].

Element	**Composition Range (%)**
Nickel (Ni)	2 - 22
Chromium (Cr)	0.5 - 10
Molybdenum (Mo)	0.5 - 3.5
Carbon (C)	0.05 - 0.50
Manganese (Mn)	0.5 - 2.0
Silicon (Si)	0.1 - 1.0

in smaller amounts to enhance specific properties.

2.6.2 Microstructure

Steels alloyed with Nickel-Chromium-Molybdenum (Ni-Cr-Mo) typically consist of ferrite and pearlite in varying proportions depending on the specific alloy composition and processing history. The addition of Ni, Cr, and Mo in steel results in the formation of several microconstituents, such as martensite, bainite, and fine carbide precipitates within the ferrite. The distribution, size, and shape of these microstructural constituents are also important parameters affecting the mechanical properties.

2.6.3 Mechanical Properties

Ni-Cr-Mo alloy steels exhibit a combination of high strength, toughness, and wear resistance. Their mechanical properties can vary significantly based on the heat treatment and the specific composition of the alloy. **Strength**: These steels exhibit high yield strength and tensile strength due to the presence of hard phases such as martensite and fine carbide precipitates. It Typically ranges from 600 MPa to 1,200 MPa or higher. **Toughness**: The presence of softer phases such as ferrite and pearlite along with the ductility provided by nickel enhances the toughness of these steels which makes them withstand high-stress applications. **Hardness**: High hardness is achieved through heat treatments such as quenching and tempering, which result in the formation of hard martensite. Hardness values can range from 30 HRC to over 60 HRC. **Ductility**: The ductility of these steels can be improved through heat treatments such as annealing and normalizing, which promote the formation of ferrite and pearlite.

2.6.4 Corrosion Resistance

Ni-Cr-Mo steels are highly resistant to corrosion, making them suitable for applications in aggressive environments, such as chemical processing, oil and gas, marine, and power generation industries. They offer:

- General corrosion resistance: These steels resist corrosion in various atmospheres and are often immune to localized attack.
- Resistance to pitting and crevice corrosion: The presence of chromium and molybdenum provides excellent resistance to localized corrosion in chloride-containing environments.
- Resistance to stress corrosion cracking (SCC): Ni-Cr-Mo steels exhibit good resistance

to SCC, making them suitable for applications involving exposure to corrosive environments under stress.

2.6.5 Wear Resistance

Ni-Cr-Mo alloy steels have good wear resistance due to their high hardness and the presence of carbide precipitates, which are resistant to deformation and fracture. The wear resistance can be further improved through heat treatments that increase hardness and through processes such as carburizing and nitriding, which increase surface hardness. Properties of Ni-Cr-Mo alloy steels can be influenced by several factors:

Composition: The specific amounts of Ni, Cr, and Mo in the alloy can influence the mechanical properties and wear resistance. For instance, increasing the amount of Mo can improve strength and hardness.

Heat Treatment: The choice of heat treatment can greatly affect the microstructure and hence the properties of the steel.

Processing Conditions: Other processing conditions such as deformation rate during forming processes can also affect the final properties of the steel [17].

Chapter 3

Wear behavior

3.1 Introduction

Wear is used to describe the damage that occurs on the surface of one or more solid objects when they are in contact and experience relative motion. Different wear mechanisms can result in distinct patterns of wear. It is possible for a surface to be affected by multiple wear mechanisms simultaneously. For instance, a surface may undergo both adhesive and corrosive wear, abrasive and fatigue wear, or a combination of several wear mechanisms. The process of wear is not static and can evolve over time or in response to changes in operational conditions. Factors such as load, temperature, lubrication, and environmental conditions can influence the wear process. Consequently, the nature and extent of wear may vary continuously. Understanding these dynamics is crucial for implementing effective maintenance strategies and minimizing surface damage to prolong the lifespan of components. Frictional heating and the resulting chemical and mechanical interactions often accelerate the process of wear.

3.2 Wear modes

Mechanical wear refers to wear primarily driven by processes such as deformation and fracturing. In ductile materials, the overall wear is significantly influenced by the deformation process, while in brittle materials, the fracturing process plays a major role in wear.
Chemical wear, on the other hand, is primarily governed by the growth rate of a chemical reaction film. This film's growth rate is mechanically accelerated by friction, leading to its designation as "tribochemical wear."
Thermal wear refers to the type of wear that is primarily influenced by local surface melting due to frictional heating. Thermal wear also includes diffusive wear, which becomes more prominent under elevated temperature conditions. Furthermore, the wear of brittle materials caused by fractures resulting from thermal shocks can be categorized as a form of thermal wear.
While these three categories of wear are crucial for providing a comprehensive characterization of wear, it is important to note that they alone are insufficient for the development of wear models aimed at predicting wear rates [1].

3.3 Wear mechanisms

3.3.1 Friction wear

Friction wear is a special wear process that occurs at the contact zone between two materials under load and subjected to slight relative movement due to vibrations or another force. In friction wear, metal-metal interfaces are essentially fixed. Debris is retained at or near the locations where it was originally formed. This debris is typically composed of metal oxides from the contacting surfaces. As oxidized debris is generally much harder than the surfaces from which it originated, it often acts as an abrasive agent that increases the friction rate. To mitigate or minimize the intensity of wear, it is advisable to employ surfaces with varying types or hardness levels, ensure sufficient movement amplitude for effective debris removal at the contact interface, and utilize high-viscosity lubricants, particularly under high contact pressures.

3.3.1.1 Types of friction wear

Sliding friction

Sliding friction is a force that opposes relative motion between solid surfaces in contact. It arises from intermolecular forces and affects mechanical system operation. It is influenced by factors like materials, temperature, and lubrication. The force to initiate motion is static friction, while opposing motion is kinetic friction. The coefficient of friction quantifies the frictional forces, defined as the ratio of frictional force to the normal force between surfaces [2].

Rolling friction

Rolling friction is a resistive force that acts in the opposite direction of the intended motion of a rotating object. It arises when there is relative motion or slip between the rolling elements. Despite this slip, the overall effect is characterized by rolling rather than sliding. Rolling friction is quantified by a coefficient of friction, which is mathematically equivalent to the coefficient of sliding friction. It is determined by dividing the resisting force acting on the rolling member by the normal force exerted on the same member [2].

Static friction

Static friction for metals refers to the force that resists the initiation of motion between two metal surfaces that are in contact and at rest relative to each other. It is the frictional force that must be overcome to set an object made of metal in motion when it is resting on another metal surface [2].

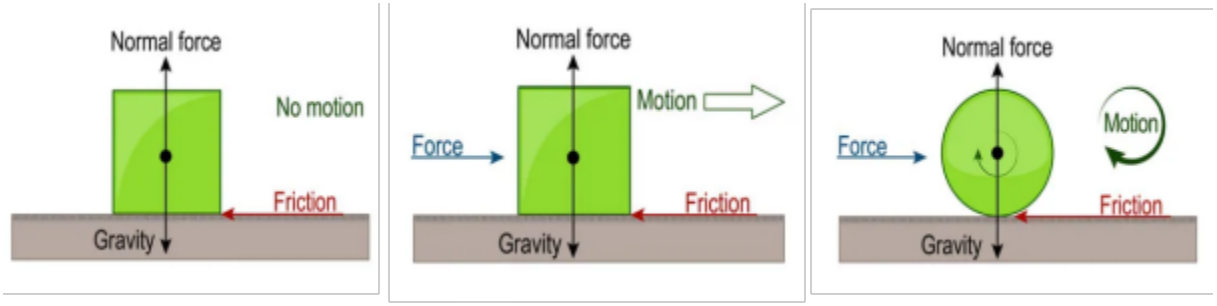

Figure 3.1: Different types of friction wear a) Static friction b) Sliding friction c) Rolling friction [3].

3.3.1.2 Contacts of friction wear

Lubricated contacts

The presence of a lubricant film significantly reduces the coefficient of friction, which typically ranges between 0.2 and 0.1. There are three lubrication regimes: hydrodynamic, mixed, and boundary [4].

- **Hydrodynamic lubrication regime**
  In the elasto-hydrodynamic regime, the coefficient of friction is primarily influenced by the properties of the fluid film that exists between the two solids. Viscosity plays a crucial role in determining the coefficient of friction in this regime. The thickness of the fluid film (h) is considerably greater than the average roughness (Ra) of the contacting surfaces. This regime is typically observed in situations where the applied normal force is relatively low and the lubricant used has a high viscosity. Lubricated contacts often operate in this regime due to its ability to minimize wear [4].

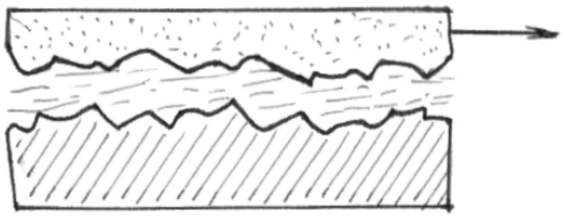

Figure 3.2: Schematic of the hydrodynamic lubrication regime [4].

- **Mixed lubrication regime**
  If the normal force increases, or if the lubricant viscosity becomes insufficient, the contact enters a mixed lubrication regime. The liquid film then has a thickness comparable to the average roughness of the surface, and some asperities come into contact [4].

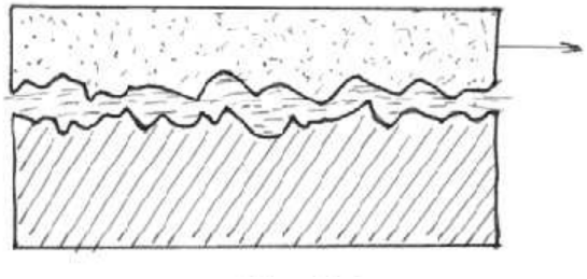

Figure 3.3: Schematic of the mixed lubrication regime [4].

- **Limit lubrication regime**
  In this regime, the two surfaces in motion come into direct contact, resulting in a substantial contact area. In this regime, the lubricant loses its effectiveness as the average thickness of the lubricating film is significantly smaller than the surface roughness. The limit lubrication regime is typically encountered when the applied normal force becomes too high or when the viscosity of the lubricant is particularly low. In this regime, the friction coefficient can increase dramatically, potentially causing contact damage through seizing [4].

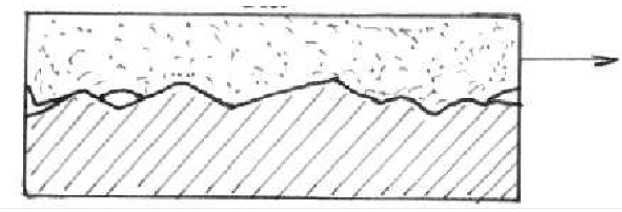

Figure 3.4: Schematic of the limit lubrication regime [4].

Non-Lubricated contacts

In order to move a solid object along a flat surface, an applied force equal to or greater than the frictional force F is required. The frictional force acts parallel to the surface and opposes the motion of the object [4]. Its intensity is proportional to the normal force F_N,

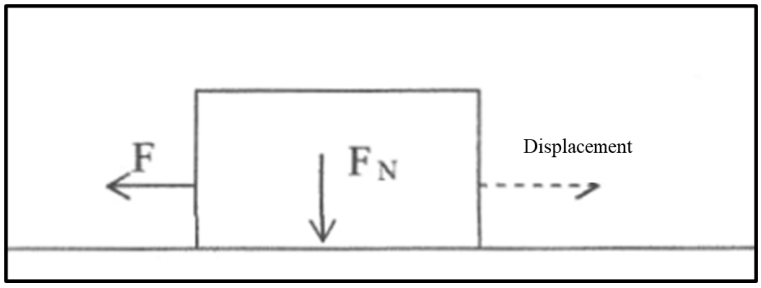

Figure 3.5: Schematic of the non-lubricated contacts [4].

also known as the weight, acting perpendicular to the contact surface. The proportionality factor f is called the coefficient of friction.

$$F = fF_n \tag{3.1}$$

The coefficient of friction is a property of the system in contact, and its value depends, among other factors, on:

- Mechanical factors: normal force, velocity of movement, viscosity of the lubricant.
- Chemical factors: humidity, oxidants, additives.
- Material properties: hardness, plasticity, surface energy.

During friction between two rough solids, three distinct physical phenomena result in energy losses and also affect the coefficient of friction:
Formation and breaking of adhesion bonds The contact between two rough surfaces of ductile metals, as shown in Figure 3.6, involves the formation and breaking of adhesion bonds. The contact is primarily limited to the contact points of the surface asperities. In this friction model for unlubricated metal surfaces, it is assumed that the harder material remains undeformed.

$$f = \frac{\tau}{H} = \frac{F}{F_n} \tag{3.2}$$

where:
τ Shear strength of the softer material forming the bond.
H: hardness.

It is also assumed that bond rupture happens within the softer material, rather than at the contact point. According to this classical theory, the coefficient of friction shows minimal variation among different metals and primarily depends on the ratio $\frac{\tau}{H}$, rather than the individual quantities. Additionally, this ratio exhibits only slight variations across different metals [4].

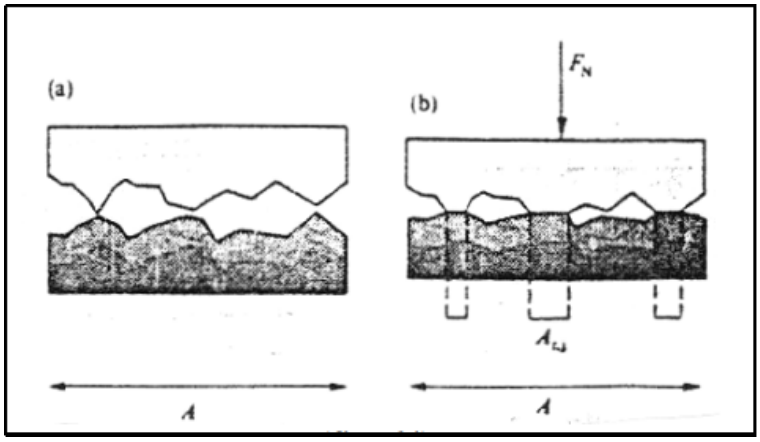

Figure 3.6: Schematic of formation and breaking of adhesion bonds phenomenon [4].

Elasto-plastic deformation of asperities According to the classical theory of friction, the initial roughness of surfaces should not affect the coefficient of friction significantly. This is because the true contact area is determined by the normal force and hardness, considering the deformation of asperities. However, in practical moving systems, there is typically an initial running-in period where the coefficient of friction is influenced by the initial roughness. This observation contradicts classical theory. When two rough surfaces slide relative to each other, the asperities undergo both elastic and plastic deformation in the direction of motion. The corresponding deformation energy contributes to the overall mechanical energy dissipated through friction [4].

Material displacement through plowing When an asperity of a hard material or an abrasive particle slide over a softer material, material displacement through plowing occurs. As a result, grooves are formed. This process requires energy and, therefore, contributes to friction [4].

3.3.2 Abrasive wear

Abrasive wear refers to the removal of metal from a surface due to the presence of hard particles or the creation of protrusions. It occurs when a hard and rough surface slides over a softer surface, sometimes referred to as grinding wear. Abrasion predominantly involves cutting and plowing processes on a small scale [5].

3.3.2.1 The mechanism of abrasive wear

Depending on the characteristics of the abrasive and wear materials, different wear mechanisms may occur, as depicted in Figure 3.7:

- Plowing: This mechanism involves the displacement of material, creating grooves without directly removing any material. Adjacent to the grooves, ridges may form, which can be subsequently removed by abrasive particles.
- Cutting: Material is directly removed from the surface in the form of primary debris or microchips, with minimal displacement to the sides of the grooves. This mechanism is similar to conventional machining processes.
- Fragmentation: Material separation occurs through cutting, and the abrasive indenter causes localized fractures in the wear material. These cracks propagate around the wear groove, leading to additional material removal through spalling.

Abrasive wear mechanisms, such as plastic deformation, cutting, and Abrasive wear mechanisms, such as plastic deformation, cutting, and fragmentation, typically occur more frequently in materials with a higher elastic modulus. This includes metals, ceramics, and rigid polymers. However, as the elastic modulus of a material decreases, the nature of the contact between the abrasive and the wear material changes. This results in localized elastic deformation becoming more significant in these situations. When there is a given length of relative motion between the abrasive and the wear surface, deeper penetration typically removes more material or causes damage to a larger volume of material. Several authors have discussed the relationship between contact pressure and wear rate in greater detail. One of the most widely accepted wear equations was developed by Archard in 1953:

$$W = Ks\frac{P}{P_m} \tag{3.3}$$

This equation states that the volume of worn (removed or disturbed) material, W, is equal to a constant, K, which is related to the probability of surface contact and debris formation,

multiplied by the sliding distance, s, the applied load, P, and the flow pressure, Pm, which is related to the hardness of the wearing surface [5].

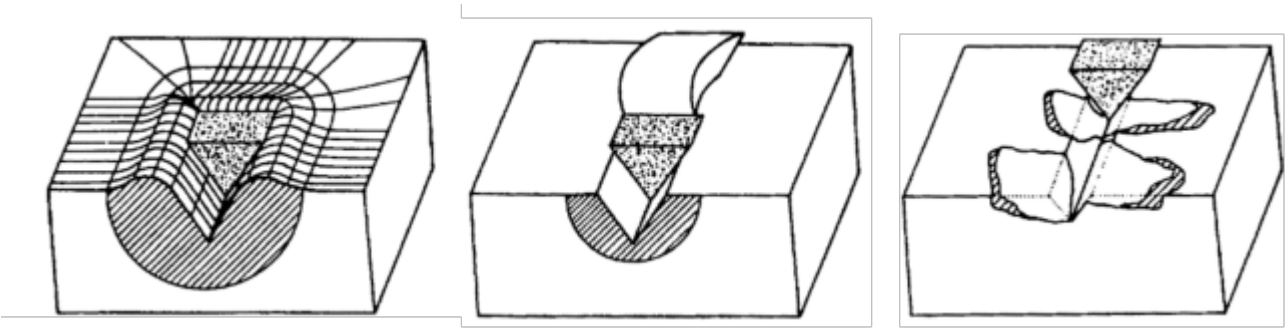

Figure 3.7: Microscopic mechanisms of material removal between abrasive particles and the surface of materials where a: Micro-plowing, b: Micro-cutting, c: Micro-cracking [5].

3.3.2.2 Factors influencing abrasive wear behavior

The majority of factors that affect abrasive wear behavior for both the abrasive and wear material are associated with their respective mechanical properties. Additionally, the mechanical aspect of the interaction between the abrasive and wear material is crucial. Chemical processes such as corrosion or oxidation are also significant as they directly impact the rate of wear of a material in the relevant environment, these factors are:

- Abrasive properties: Particle size, particle shape, Hardness, Yield strength, Fracture properties and concentration.
- Contact conditions: Force/impact level, Velocity, Impact/impingement angle, Sliding/rolling, Temperature, Wet/dry, pH.
- Wear material properties: Hardness, Yield strength, Elastic modulus, Ductility, Toughness, Work-hardening characteristics, Fracture toughness, Micro-structure, Corrosion resistance [5].

3.3.3 Fretting corrosion

Fretting corrosion is a form of damage that arises when two metal surfaces in motion come into rubbing contact, particularly when the lubricant is not adequately replenished, leading to corrosion at those points. This phenomenon primarily occurs when the interface experiences vibrations (repetitive movement between the two surfaces) and compressive loads [7].

Adhesion takes place during this process, which is generally regarded as more severe than false brinelling. Typically, it manifests as a reddish-brown oxide hue (similar to rust in the absence of water) on steel and a black color on aluminum, generating metal wear debris flakes that are either formed or shed off [8].

3.3.3.1 Fretting corrosion mechanism

To provide a very brief analysis of fretting corrosion, let us consider the common scenario of two ferrous metal pieces resting on each other and subjected to vibrations. Three main phenomena take place:

- During the displacements, the surface roughness of the metals in contact adhere together, potentially leading to welding. This results in the detachment of very fine metallic particles. It is a mechanical action of detachment.
- The exposed metal beneath the detached roughness quickly oxidizes. Similarly, the detached metallic particle undergoes oxidation. This leads to the formation of iron oxide, Fe2O3, a red-colored product that is non-hydrated and distinct from rust. We are witnessing a chemical action of oxidation.
- Contrary to typical friction, the detached and oxidized particles remain in place and act as abrasives. Fe2O3 exhibits a high abrasive power. This represents a mechanical action of abrasion.

These three actions, two mechanical and one chemical, combine to rapidly deteriorate the contacting surfaces. Additionally, surface cracks may form, propagate, and ultimately lead to fatigue failure of the component [9].

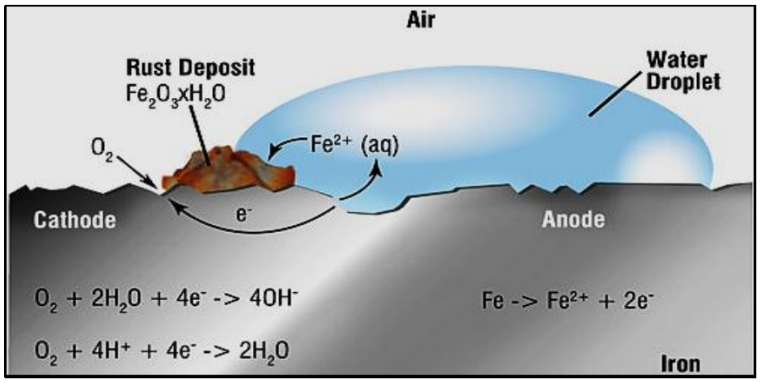

Figure 3.8: Schematic illustration of fretting corrosion mechanism [10].

3.3.3.2 Factors influencing fretting corrosion

Factors influencing fretting corrosion are numerous and can be classified to three categories: Operating conditions, Materials used, and The Lubricant used

Operating conditions

The parameters of operating conditions that have an influence on fretting corrosion are listed and discussed below:

- **Vibration amplitude**
  Vibration amplitude may be the primary factor in many cases. Small amplitudes appear to be the most hazardous, with relative displacements between components ranging from 0.01 to 0.2mm and slight rotation in bearings. Larger amplitudes, on the other hand, are generally less dangerous which is explained by the evacuation of oxidation products, resulting in reduced abrasion.

- **Temperature**
  When temperature decreases lubricant penetrates the surface less effectively, and at high temperature, fretting corrosion decreases. The given explanation is that the abrasive Fe3O4 forms only at low temperatures, whereas at high temperatures, FeO and Fe2O3, which are less dangerous, are present. However, if the lubrication factor is eliminated, it can be said that between 0°C and 80°C, temperature has little influence on this type of damage.

- **Load**
  An increase in load can have a beneficial effect if it leads to the suppression of vibrations. Conversely, it can have a detrimental effect if it does not affect the vibrations and increases the contact surface, as is the case with bearings. In general, an increase in load tends to increase the extent of damage.

Material used

The phenomenon of contact corrosion can occur with almost all materials, including glass, ruby, and plastics. Heat treatments do not seem to have notable effects, and the phosphatization of steel surfaces has a similar outcome. On the other hand, anodization of aluminum surfaces and sulfo- nitriding of steel surfaces are clearly beneficial for resistance to contact

corrosion. A very slight surface roughness, as long as it allows better penetration of lubricant, promotes resistance to contact corrosion. However, in all other cases, a good finish is preferable.

Lubricant

Lubricants can play a significant role to prevent contact corrosion. Like in many applications, two factors are important: the quality and quantity of the lubricant used.

- **Oil**
  If the oil only reaches the contacting surfaces in small quantities, a fluid oil that penetrates better than a viscous oil gives better results. However, if the component is immersed in oil or generously lubricated, a viscous oil will provide better protection by creating a film that is more resistant to impacts and vibrations than a fluid oil.
- **Grease**
  To be effective, a grease must possess two essential characteristics: It should contain a fluid oil, and it should have a relatively low consistency.

When at rest, grease is a plastic substance that cannot penetrate between the contacting surfaces. Therefore, it is believed to be important for oil to escape from the grease and penetrate between the surfaces. Since the amount of oil released by the grease can only be small, it is necessary for this oil to be fluid [9].

3.3.3.3 Preventive methods

Complete prevention of fretting wear damage typically involves separating the contacting surfaces. Other approaches, such as lubrication, improving the fit or changing materials, can delay the onset of fretting and slow down surface deterioration. Applying coatings to surfaces experiencing fretting is usually considered when challenges arise in fabricating a complete component from the coating material, or when the associated costs are prohibitive [11].

Change in design Design optimization is a common approach to suppress fretting, which typically involves modifying the geometry of components and selecting different materials for contact surfaces. However, it is important to note that redesigning is not always feasible due to the associated costs and time constraints. Moreover, these measures can sometimes introduce issues such as overloading or a decrease in fatigue strength [12].

Application of surface treatment Coatings can be used to prevent fretting corrosion by

providing a protective layer between the two surfaces in contact. For example, coatings containing oxides of iron and chromium can reduce the coefficient of friction. Dilute nickel alloy coatings, on the other hand, contain only minor amounts of oxides and are soft, which means that metal-to-metal contact occurs soon and adhesion and tearing results. Composite coatings behave similarly to steel coatings in the early stages, probably because of the presence of Fe-Cr oxides between particles [11].

3.3.4 Impact wear

Impact wear occurs due to repeated collisions between two surfaces in contact. This type of wear typically involves flat or nearly flat surfaces with a relatively large radius of curvature compared to the size of the resulting wear scar. This characteristic sets impact wear apart from erosive wear, which occurs when a sharp particle indents a flat surface. In the case of impact wear, the surface experiences repetitive impacts from a series of high-stress pulses, accompanied by some energy dissipation during each impact. Figure 3.9 provides a schematic representation of this phenomenon.

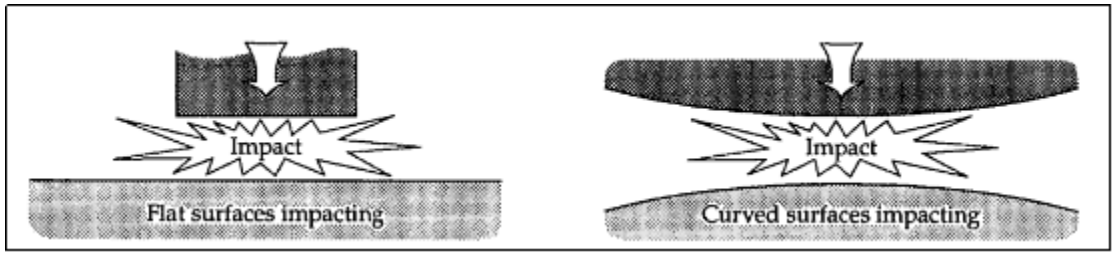

Figure 3.9: Schematic illustration of repetitive stress pulses under impact wear [13].

When the impact energy is high, elastic and plastic deformation occurs, and/or fatigue is followed by wear debris release as a result of crack formation. A corrosive or oxidative wear process can also occur if oxygen is available and the wearing substance can be oxidized. Iron and steel parts are prone to tribo-oxidation impact wear, especially at high temperatures when oxidation happens quickly. In general, impact wear depends on the development of distorted layers, especially when fatigue or crack formation is the main cause of wear. Due to contact forces upon impact, the material through which the cracks spread is frequently plastically deformed and work-hardened [13].

3.4 Wear behavior of structural steel

One of remarkable structural steel classes is High-strength low-alloy (HSLA); they are known for their excellent wear resistance properties. These steels possess a unique combination of high strength and enhanced resistance to wear, making them highly desirable for a range of applications. With a carefully designed microstructure and alloying elements, HSLA steels exhibit superior performance in abrasive environments. Their wear resistance surpasses that of carbon steels due to the addition of specific alloying elements and the utilization of appropriate heat treatment techniques. By incorporating HSLA steels, industries can benefit from their remarkable ability to withstand wear and extend the service life of components exposed to demanding conditions.

3.4.1 Factors influencing wear behavior

The wear behavior of HSLA steels depends on factors such as chemical composition, microstructure, hardness, and surface conditions. Some key factors influencing wear behavior in HSLA steels include:

- **Hardness**: Higher hardness generally provides better resistance to wear. The hardness of HSLA steels can be enhanced through heat treatment processes such as quenching and tempering.
- **Microstructure**: The presence of various microstructural constituents, such as ferrite, pearlite, and bainite, can affect wear resistance. Fine-grained microstructures tend to exhibit better wear resistance.
- **Alloying Elements**: The addition of alloying elements like manganese, silicon, vanadium, and niobium can improve wear resistance by enhancing the hardness, toughness, and work-hardening ability of the steel.
- **Surface Conditions**: The surface finish and texture of the steel can influence its wear behavior. Surface treatments such as shot peening or coatings like nitriding can improve wear resistance [14].

3.5 Experimental methods for wear testing

Standard wear testing methods have limitations and may not always provide an accurate representation of wear rates in real-world applications. Wear mechanisms can vary depending on the specific circumstances involved. When selecting a suitable test method for a particular type of wear, several factors should be taken into account. It is preferable to choose a test that is efficient, controllable, allows for continuous measurement of friction and wear, cost-effective, repeatable, and provides enough data for statistical accuracy. Ideally, the chosen test method should closely mimic the real-world conditions, where the wear type and environment are similar to those encountered in the actual application. The wear rate observed on the test specimen should align with the wear exhibited by the "real" worn material on both macroscopic and microscopic scales [15].

3.5.1 Tribological test

Tribology is an interdisciplinary science that integrates knowledge from diverse fields such as physics, mechanical engineering, materials science, and chemistry. It focuses on the study of phenomena that occur when two bodies come into contact and are in motion. By drawing from multiple disciplines, tribology offers a holistic approach to understanding these phenomena. The field of tribology encompasses various theories and models that explain the physical processes at the interface of contacting surfaces. These theoretical frameworks, supported by mathematical models, enable tribologists to analyze and predict friction, lubrication, wear, and other tribological phenomena. The theories incorporate principles from classical mechanics, thermodynamics, surface science, and contact mechanics, among others. Through the application of these theories and models, tribologists gain insights into the underlying mechanisms and behaviors of systems, facilitating the development of effective strategies for reducing friction, improving lubrication, and minimizing wear in practical applications [16].

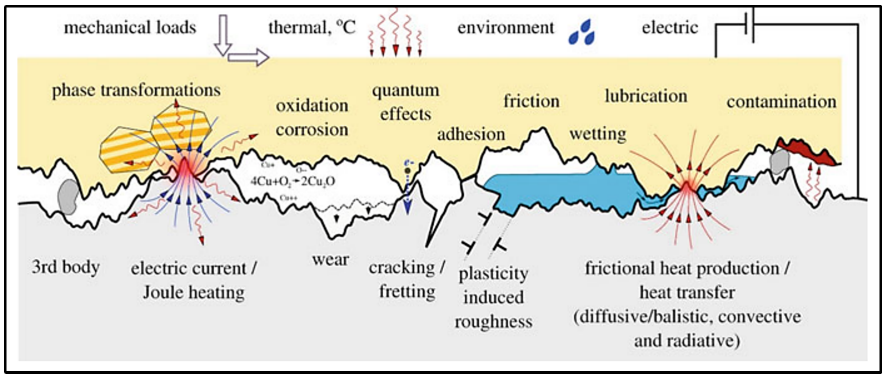

Figure 3.10: Multiphysical nature of tribology: two bodies make contact when exposed to various loads: mechanical, thermal, electric, and environmental [16].

3.5.1.1 Tribometer

Tribometer, also known as a tribotester, is a versatile device used to simulate and study friction and wear between surfaces. It plays a crucial role in tribology research and development, allowing scientists and engineers to investigate material behavior, understand friction and wear mechanisms, and evaluate the effectiveness of surface treatments and coatings. Tribometers enable precise control of experimental parameters such as load, speed, temperature, and environment, ensuring reproducibility and facilitating comparative studies. These devices consist of specimens or samples that come into contact and slide against each other, generating frictional forces. They provide valuable data and measurements including friction coefficients, wear rates, surface roughness changes, and contact pressure distributions. This information helps characterize the tribological properties of materials and lubricants, assess their performance under different conditions, and guide the design and optimization of surfaces and lubrication systems. Different types of tribometers exist, such as pin-on-disk, ball-on-disk, and reciprocating tribometers. Pin-on-disk tribometers are particularly prevalent in tribology research and find applications in various industries like automotive, aerospace, manufacturing, and biomedical. They feature a stationary pin and a rotating disc, allowing for controlled testing and evaluation of materials and lubricants. The versatility and precision of tribometers make them invaluable tools for improving the efficiency, reliability, and lifespan of mechanical systems [17].

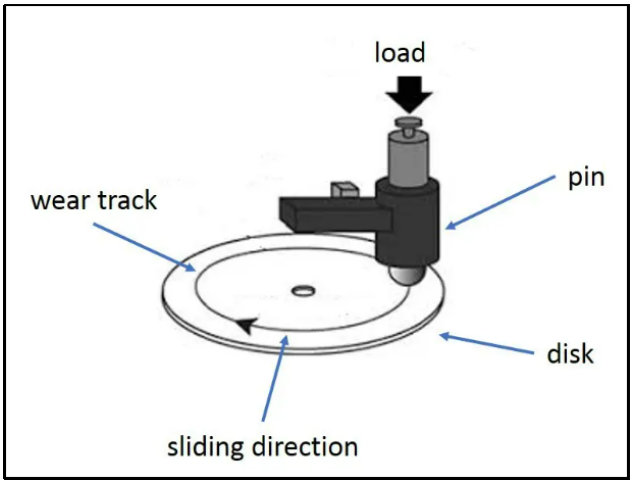

Figure 3.11: Schematic of pin on disc tribometer [16, 17].

3.5.1.2 Impact wear tester

An impact wear tester, commonly known as a hammer impact wear tester, is a specialized equipment used to evaluate the resistance of materials to impact wear. It is particularly useful for studying the wear behavior of components subjected to high-velocity impacts. The key components of an impact wear tester include:

- **Hammer Assembly**: The hammer assembly consists of a weighted hammer or striker that delivers controlled impacts onto the test specimen. It is designed to replicate the impact forces encountered in real-world scenarios.
- **Clamping Chuck**: The clamping chuck securely holds the test specimen in place during the impact test. It ensures that the specimen remains stationary and properly aligned for accurate and consistent impact measurements.
- **Test Specimen**: The test specimen, typically in the form of a small sample or disc, is the material being evaluated for impact wear resistance. It is clamped onto the chuck and positioned directly beneath the hammer assembly.
- **Down Specimen or Anvil**: The down specimen, also known as the anvil, serves as the receiving surface for the impacts from the hammer assembly. It is positioned below the test specimen and provides a stable platform to measure the wear caused by the impacts.
- **Measurement System**: An impact wear tester incorporates a measurement system to quantify the wear and damage caused by the impacts. This may include optical sensors, profilometers, or other instruments capable of assessing wear depth, wear volume, or changes in surface roughness.

- **Control System**: The impact wear tester is equipped with a control system to regulate the impact parameters such as impact velocity, impact force, and test duration. This ensures consistent and repeatable testing conditions.

During the test, the hammer assembly strikes the test specimen with controlled impacts, simulating the impact wear experienced in real-world applications. The resulting wear on the test specimen is measured and analyzed to evaluate its impact wear resistance. Impact wear testers are widely used in industries such as mining, construction, and automotive, where materials are exposed to repeated impacts from abrasive particles or surfaces. By studying the wear behavior under controlled conditions, researchers and engineers can make informed decisions about material selection, design improvements, and protective coatings to enhance the durability and reliability of components in demanding environments [18].

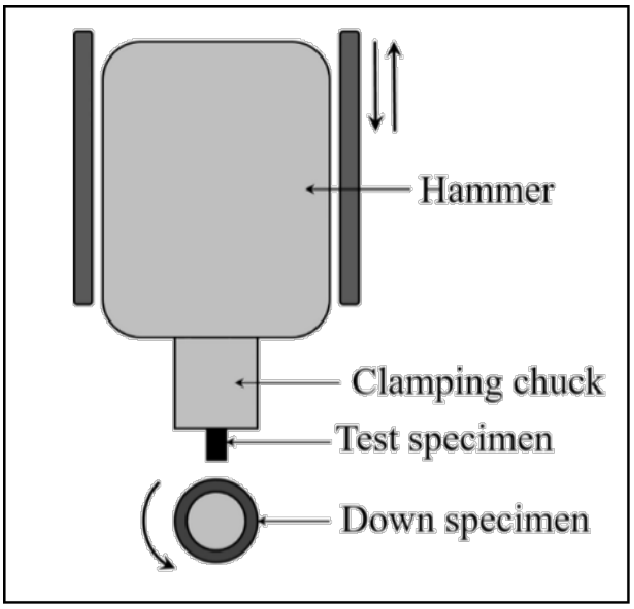

Figure 3.12: Schematic of impact wear tester [18].

Second part

Experimental study

Chapter 4

Experimental procedures

4.1 Chemical analysis

4.1.1 Objective

We aim to conduct a chemical analysis in order to identify the elemental composition of steel samples, providing us with valuable insights into their properties. Subsequently, we will compare the results obtained with reference materials to estimate the grade and type of steel that we're studying in this project. Moreover, the obtained elemental composition will serve as a foundation for further investigations which will facilitate a more comprehensive understanding of the steel's properties and behavior.

Figure 4.1: SpectroMaxx machine.

4.1.2 Experimental procedure

To perform chemical analysis of the steel samples, we utilized Optical Emission Spectroscopy (OES) with a SpectroMaxx machine (Figure 4.1) from ORFEE BCR Group. The general experimental procedure is outlined below:

- **Sample Preparation**: Initially, we cut the lower part of the Pin to obtain a flat surface that was sufficient to cover the emitted arc. It was later on cleaned alongside with the Insert to remove any contaminants that may affect the analysis
- **Calibration Standards**: Calibration standard is prepared using the steel grade of 30CrNiMo8 as a reference to compare results. Our objective is to establish a range of concentrations that encompasses the expected carbon concentrations in our steel sample, which is less than 0.3%.
- **Sample Analysis**: The prepared steel sample is placed in a suitable sample holder, ensuring good contact with the instrument to perform measurements during a sufficient integration time for accurate spectral acquisition.

We repeated the analysis many times for each sample to ensure reliability and statistical significance. Results are obtained at the end in a comprehensive report summarizing the analysis, including sample details, and methodology.

4.2 Metallographic study

Metallography is a field of study that focuses on examining and analyzing the microstructure of different metallic alloys. It employs a scientific approach to observe and determine the chemical and atomic structure, as well as the spatial distribution of grains, constituents, inclusions, or phases within metallic alloys. Furthermore, the principles of metallography can be extended to characterizing other materials too. In our case, it serves as the initial step in a series of experiments. The analysis of a material's microstructure is vital for assessing the accuracy of its processing, making it a critical consideration across various industries. To conduct a comprehensive metallographic examination, several essential steps must be followed. These steps include sampling, specimen preparation (sectioning, cutting, mounting, planar grinding, rough and final polishing, and etching), microscopic observation, digital imaging and documentation. By adhering to these procedures, precise and detailed information regarding the material's microstructure can be obtained for further analysis and evaluation.

4.2.1 Sample preparation

The first stage of metallographic analysis, known as sampling, is of utmost importance as it directly impacts the reliability and validity of any subsequent study. It is crucial to choose a specimen that accurately represents the material being evaluated. In our case, the pieces were too small and challenging to be cut with a traditional cutting machine. As a result, we opted to use an electro-erosion machine for more precise work. The electro-erosion machine used was the DK 7745 (Robofil), as shown in Figures 4.2 alongside with our samples after being cut.

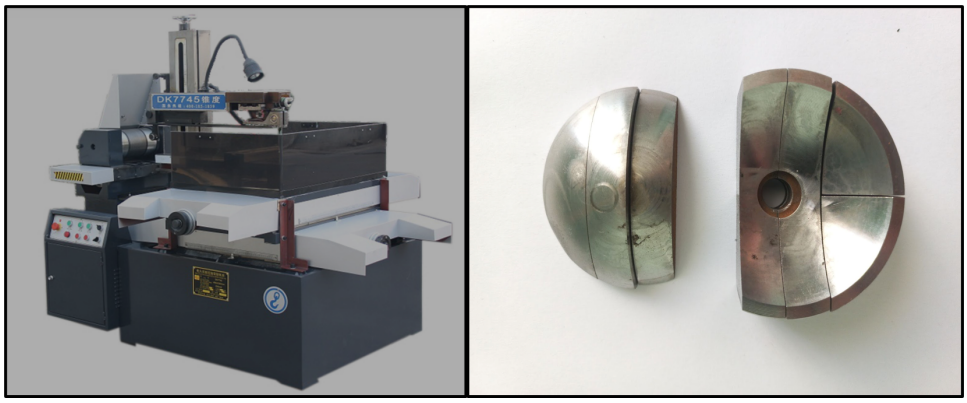

Figure 4.2: a) DK7745 electro-erosion machine, b) sectioned samples.

4.2.2 Heat treatment

The objective of this heat treatment experiment is to enhance the hardness of steel samples through the process of austenitizing, quenching, and tempering in the Nabertherm oven. By subjecting the samples to specific heat treatment parameters, we aim to achieve a desired level of hardness. This experiment will contribute to the knowledge of heat treatment techniques for improving the hardness of steel.

Austenitizing

To begin the experiment, we obtained three steel samples, shaped in right circular cylinder with a diameter of 5cm and a height of 2cm. The oven was preheated to a temperature of 880°C. when reaching the desired temperature, steel samples were carefully placed inside the oven, by making sure they are evenly spaced and not in contact with each other or any surfaces within the oven. We closed the oven door securely allowing the samples to remain inside the preheated oven for a period of 40 min to achieve austenitization.

Quenching

After the desired austenitization time has elapsed, we opened the oven door and quickly transferred the steel samples using crucible tongs to a container filled with water, ensuring they are fully submerged. This rapid quenching process will help to rapidly cool down the samples and achieve the desired hardness. Steel samples remained in the water for a sufficient period of time to complete the quenching process, typically from a few seconds to a minute. Once the quenching process is complete, we removed the steel samples from the water and dry them using a clean, dry cloth.

Tempering

The ultimate step involved preheating the Nabertherm oven to a temperature of 500°C, then placing the quenched steel samples back inside the oven, ensuring they are properly spaced. After closing the oven door allowing the samples to temper at 500°C for one hour. Once the tempering time has elapsed, we turned off the oven and removed the steel samples to cool

down in the air to room temperature.

Figure 4.3: Nabertherm oven used for austenitizing and tempering.

4.2.3 Hot Coating

After the preparation stage, it is recommended to apply a hot coating to the samples. To accomplish this, we utilized the METAPRESS-A enrober and followed the following steps:

- Melting the coating resin: Once the samples are placed in the enrober, ensuring that the desired face is positioned downwards to prevent coating, we proceeded to melting the resin at an appropriate temperature.
- Cooling: After the coating process, we cooled the samples using the water connection of the enrober. Once they get adequately cooled, we removed them from the enrober.

Figure 4.4: METAPRESS-A Enrober.

4.2.4 Polishing

Polishing is a critical step in the metallographic sample preparation process, where a series of sequential steps are followed to achieve a smooth, scratch-free, and highly reflective surface. We began the polishing process using abrasive discs with varying grit sizes, starting from P120 and progressing up to P2400. This gradual refinement helps eliminate deformations and scratches on the sample surface. Depending on the specific requirements, the polished samples may undergo examination in either their etched or unetched state, which reveals the steel's microstructure. However, we encountered a challenge during the polishing stage. We noticed that rust formation occurred instantly on the samples, requiring us to periodically wash them with ethanol to remove the rust and maintain the sample quality. After addressing the rust issue, we proceeded to further refine the samples by using alumina on a felt paper. This final step aimed to achieve a mirror-like finish on the sample surfaces, enhancing their reflectivity and facilitating accurate microscopic observation.

Figure 4.5: MECATECH Z64 Polishing machine.

4.2.5 Etching

Depending on the specific phase and the composition of the metallic matrix, various chemical or electrolytic etchants are available for metallographic analysis. In the case of steels, etchants such as Nital, Murakami, Kaling, and sodium hydroxide (NaOH) can be used. The duration of the etching process is a critical parameter that affects the accuracy of the measurement, as it determines the level of clarity in quantifying the desired phase. Adjusting the etching time allows for the distinct revelation of the phase of interest, enabling more precise quantification. For our case, we opted to use a 4% Nital etchant with the following conditions: 0.4ml of Nitric acid mixed with 9.6ml of ethanol. The etching process was conducted for a duration of 12 seconds.

4.2.6 Optical Microscopic observations

Optical microscopy is a widely used technique for visualizing the microstructure of various materials. It involves the use of light to examine objects at a microscopic level. An optical microscope, also known as a light microscope, utilizes lenses and light sources to magnify and illuminate the sample, allowing for detailed observation and analysis. The basic components of an optical microscope include objective lens, an eyepiece, a light source, and a stage for holding the sample. The objective lens collect and magnify the light passing through the sample, while the eyepiece further magnifies the image for the observer. The light source provides illumination, which can be transmitted through the sample (transmitted light microscopy) or reflected off the sample (reflected light microscopy). To visualize the microstructure of our material, we positioned the sample on the microscope stage and adjusted the objective lens to focus on the specific region of interest. To capture detailed micrographs, we utilized different magnifications, including x50, x100, x200, x500, x1000, and x1500. Each magnification allowed us to examine the material at varying levels of detail, providing a comprehensive understanding of its microstructural features.

Figure 4.6: Nikon Optical microscope.

4.2.7 Scanning Electron Microscopy SEM

The objective of utilizing Scanning Electron Microscopy (SEM) was to closely observe the surface of our steel samples for any defects, cracks, or surface treatment and employ Energy-Dispersive X-ray Spectroscopy (EDS) to analyze their elemental composition, the SEM used was FEI Quanta 650 from the Research center and development CRD.

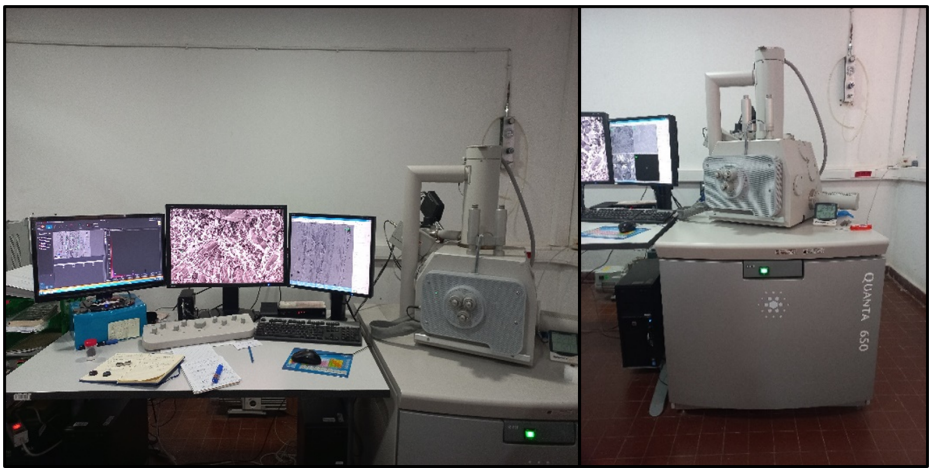

Figure 4.7: Quanta 650 Scanning Electron Microscope.

For our analytical work, we proceeded as follows: The prepared steel sample was mounted onto SEM stubs using carbon tape, and then inserted into the SEM chamber. The SEM parameters we used are 15 KV acceleration voltage and working distance, spot size were optimized for surface imaging. The surface of the steel sample was observed using high-resolution imaging modes including secondary electron imaging (SEI) or backscattered electron imaging (BEI), to capture detailed surface morphology.

EDS Analysis: the SEM is equipped with an EDS detector so that after obtaining SEM images of the steel surface, we employ the EDS technique for elemental analysis. This method

utilizes the interaction of X-rays with the sample to determine the elemental composition of selected areas of interest on the steel surface. X-ray spectra were acquired, and the detected X-ray signals were processed to identify and quantify the elements present on the surface. By combining SEM observation with EDS analysis, we aimed to identify the surface morphology and elemental composition of the steel samples, contributing to a better understanding of their structure and properties.

4.3 Hardness measurements

The hardness test is a mechanical test used to determine the hardness of a material, which is a measure of its resistance to indentation, scratching, or deformation. Principally, we proceeded to this testing on both thrust pin and insert to determine their mechanical properties, such as strength, wear resistance, toughness, and durability. Furthermore, we performed multiple tests in the laboratories of the following three organizations: CRTI of Chéraga, BCR of Bordj Mnaeil, and ATP Mesrouk of Blida.

4.3.1 Experimental procedure

Before proceeding, we ensured that samples are clean, flat, and have a smooth surface, with no contaminants or surface irregularities that may affect the hardness measurement. After that, with the help of the laboratory engineer, HV and HRc hardness were measured using INNOVATEST NEMESIS 9000 Vickers hardness machine (Figure 4.8) and MITUTOYO Rockwell hardness testing machine (Figure 4.9).

4.3.1.1 Vickers hardness test

The Vickers hardness test involves using a diamond indenter shaped as a right pyramid with a square base and opposite faces at a 136-degree angle to make an indentation on the sample executing the following steps:

- **Positioning**: the pin/insert sample is placed on the test stage of the hardness tester and positioned so that the desired testing area is directly beneath the indenter.
- **Initial Load**: initial load is applied to the indenter to establish contact with the sample surface.
- **Dwell Time**: the initial load is maintained for 10 seconds to ensure proper indentation formation.

- **Final Load**: final test load of 10 Kgf is applied and maintained for the specified dwell time.
- **Unloading**: the test load is then released and removed from the steel surface, allowing the sample to return to its original shape.
- **Measurement and calculation**: Measuring the diagonals of the diamond-shaped indentation using a microscope gives the vickers hardness value calculated systematically and reported as of 200 HV/10 referring to a Vickers hardness of 200, was obtained using a 10 kg force.

Figure 4.8: INNOVATEST Vickers hardness equipment.

4.3.1.2 Rockwell hardness test

The Rockwell hardness test method involves using a diamond cone or hardened steel ball indenter to create an indentation on the test material. Steps for measurements are approximately the same with Vickers hardness test and are described below:

- **Positioning**: placing the sample on the anvil of the Rockwell hardness tester and ensuring it is stable and securely positioned.
- **Initial Load**: applying an initial minor load to the indenter, that is automatically pre-set to 10 Kgf which establishes contact with the steel surface.
- **Zero Setting**: the initial position of the dial gauge is set to zero to establish a reference point.

- **Major Load Application**: the full major load of 150 kgf is applied to the indenter, which penetrates the steel surface.
- **Dwell Time**: maintain the major load for a specific dwell time
- **Unloading**: Release the major load and remove it from the steel surface, allowing the sample to return to its original shape.
- **Reading and Recording**: wait until the pointers of the Mitutoyo gauge stabilize before reading the Rockwell hardness value which represents the difference in depth between the initial zero position and the final indentation depth.

Figure 4.9: MITUTOYO Rockwell hardness equipment.

4.4 Microhardness measurements

The objective of this study is to perform microhardness measurements as the final step in characterizing our steel samples. The Nikon 600 machine from CRD is used to identify variations in hardness across different regions of the steel sample, and then correlating these measurements with the observed microstructure, it becomes possible for us to establish relationships between steel properties and microstructural features.

Figure 4.10: Nikon 600 Microhardness machine.

Measuring the microhardness is similar to measuring hardness besides the presence of an integrated microscope to select the desired section for analysis, below are the steps we followed to get accurate results:

- Mounting the sample securely on the stage.
- Automatically sliding the stage while observing in the microscope screen to select the test points on the sample surface where we want to measure microhardness.
- Placing the indenter tip on the test point, and applying 10 Kgf load for a specified dwell time.
- Measuring the diameters of the indentation and recording Vickers hardness measures We repeated this process at different test points to ensure a representative assessment of the hardness across the sample.

4.5 Tribological study

4.5.1 Introduction

One of the main goals of this study is to investigate the tribological properties of the Thrust Pin and Insert. To accomplish this, we have opted to use a pin-on-disc tribometer, which is widely recognized for its availability and excellent performance in tribological research and testing. The experimental methodology of the ball-on-disc tribological test involves the systematic evaluation of friction and wear characteristics exhibited by materials in contact, under controlled test conditions. This approach is commonly employed to assess the durability and performance of different materials subjected to sliding contact scenarios. The experimental setup typically consists of a rotating disc specimen and a spherical ball-shaped counterpart that applies a specific load onto the disc surface. These components are made of materials or coatings of interest, representing the contacting surfaces found in real-world applications. The test is conducted in a controlled environment, often at ambient conditions or under specific temperature and humidity settings. During the test, the disc specimen rotates at a constant speed while the ball counterpart slides against it under a defined load. The resulting frictional forces at the interface between the two surfaces are measured and monitored throughout the test.

These force measurements provide valuable insights into the material's resistance to sliding and the efficiency of energy conversion at the contact interface. Furthermore, the wear of the contacting materials is assessed by quantifying the loss of material mass or analyzing the surface damage caused by the sliding motion. Techniques such as optical microscopy, scanning electron microscopy (SEM), and profilometry may be employed to examine the wear tracks and surface features. The experimental parameters, including the applied load, sliding speed, test duration, and environmental conditions, can be adjusted to simulate specific operating conditions or to investigate the influence of various factors on the tribological behavior of the materials. The findings derived from the ball-on-disc tribological test can be utilized to optimize material selection, develop effective surface coatings, refine lubrication strategies, and enhance overall performance in diverse mechanical systems.

4.5.2 Tribometer

The Research Centre of Industrial Technology (CRTI) offers an intriguing piece of equipment for tribological tests, known as the Universal and Versatile Ball-Disc and Linear Oscillating Tribometer. This equipment provides rotational and translational movement capabilities as required for the study.

Figure 4.11: TRIBOtechnic Tribometer

4.5.3 Materials of the pin-disc couple

For the rotational disc, we will use either the pin or the insert samples, as both of them need to be tested to analyze their performance under the same conditions. This allows for a direct comparison of their tribological characteristics.
As for the ball, it was made of a tool steel specifically designed for bearing applications. It has 5.5mm of diameter, made of low alloyed chromium tool steel with a grade of AISI 52100 (AFNOR 100C6/100Cr6). This grade of tool steel has a martensitic structure with a hardness of 60 to 66 HRc.

4.5.4 Experimental procedure

A laboratory test should aim to replicate real-world conditions as closely as possible. In our case, we have selected the following parameters for the rotational type tribology test:

- Speed: 110 mm/s.
- Duration: 30 minutes.

- Wear groove: 3 mm.
- Variable load: 4N, 6N, 8N, 10N, and 12N.
- Slip length: 200 m.
- Environmental temperature: 23 °C.

The test procedure is completely operated by the Tribotester software. To run the test, we proceeded to the following requirements:

- As the only variable for assessing wear of our sample is the applied load, we have chosen to vary it from 4N, 6N, 8N, 10N, to 12N the maximum load that can applied, an example of 10N taking into account 1N of the weight holder is shown in (Figure 4.12)
- Fix the sample on the rotational disk holder, and the ball at the end of the measuring arm.
- Enter the test parameters previously presented.
- Ensure that the ball has precise contact with the surface being tested by adjusting the measuring arm to a completely horizontal position. This adjustment will also eliminate the weight of the arm and ensure accurate application of the load.
- Launching the test will make the disk turn at the speed indicated, and two curves of friction force and friction coefficient will be drawn in real time.
- Measurement stops automatically when sliding length e.i test duration is reached.

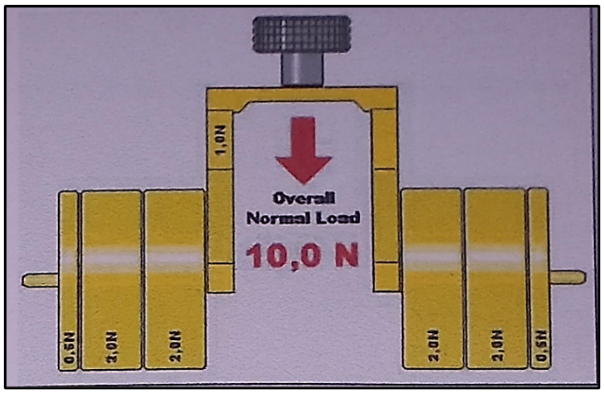

Figure 4.12: 10 N applied load

4.5.5 Wear characterization

Characterizing wear grooves after tribology tests is essential for understanding material performance. It provides insights into wear mechanisms, surface interactions, and wear resistance. By analyzing groove width, depth, and shape, we can identify wear severity and failure modes. Therefore we chose to use two technique for characterizing:

4.5.5.1 Profilometer

Profilometer is an instrument used for measuring and characterizing the surface profile or roughness of an object. It provides detailed information about the texture, smoothness, and irregularities present on a surface at a micro or nanometer scale. After the tribometer test, it is necessary to measure the depth of the wear groove in order to evaluate the extent of wear and the volume of material loss. For this purpose, the tribometer we used is equipped with a profilometer installation capable of measuring the worn surface of the track with high accuracy. The profilometer has a resolution of 7.55 nanometers in the Z-axis and is equipped with a skidless tracer with an internal reference. This allows precise measurements to be taken on samples as small as 2 mm. In contrast, a tracer with a skid requires samples of at least 35 mm in size.

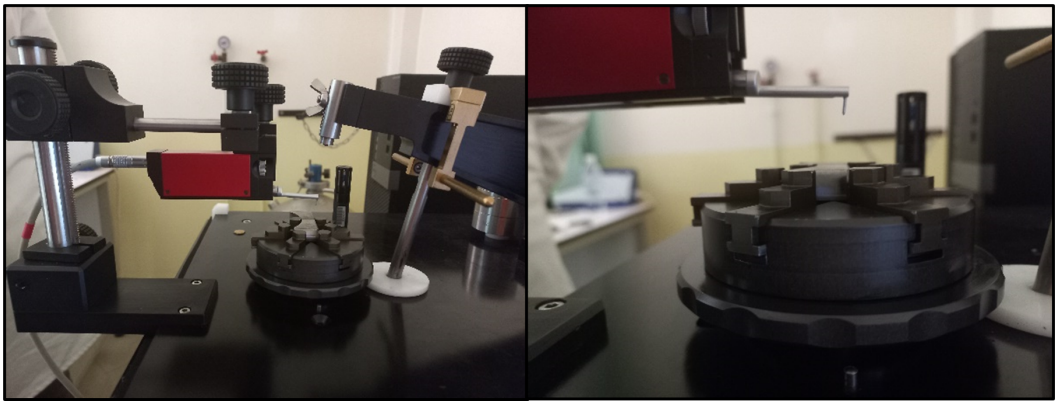

Figure 4.13: Profilometer

To use a profilometer to calculate wear depth and section in order to calculate the wear rate, we followed these steps:

- **Setting up the profilometer**: Ensuring that the profilometer is properly calibrated and aligned according to the Manuel. Making sure the probe is in good condition and properly mounted.
- **Choosing the measurement area**: we chose a specific region of interest where the wear groove has occurred on the surface of the material.

- **Starting measurement**: Positioning the profilometer probe at a reference point outside the wear region and initiating the measurement.
- **Recording profile data**: As the profilometer scans across the wear region, it will measure the surface profile at regular intervals. The data is typically recorded as a profile plot.
- **Analyzing profile data**: Using the software provided by the tribometer, the recorded profile data is processed to analyze the wear grooves. The wear depth is determined by calculating the difference between the original surface height and the lowest point within the wear region. This analysis allows for quantification of the depth of wear and provides valuable information about the extent of material loss and wear severity.
- **Calculating wear section**: Measuring the width or length of the wear region perpendicular to the direction of sliding.
- **Calculating wear rate**: The wear rate can be calculated by dividing the wear depth by the wear section. Ensuring that the units are consistent for accurate results.
- **Repetitive measurements and average**: For more accurate results, we repeated all the measurements at multiple locations within the wear region and calculated an average wear depth and section.

The profilometer generates a graph from which we can extract the wear depth and the area of the wear track section. These measurements are then provided to the software for calculating the wear rate. It is determined using the following formula:

$$K_w = \frac{S 2\pi R}{F_n 2\pi n} \tag{4.1}$$

Where:
Kw: Wear rate (m^3/N/m).
S: Track section.
n: Number of rounds.
R: Radius track.
Fn: Normal load on friction surface.

4.5.5.2 Scanning electron microscopy

The other techniques for characterizing the wear grooves is using the same SEM from CRD as it provides several benefits in analyzing and understanding results. (Figure 4.7). The primary objective of conducting SEM analysis consists of two aspects:
Surface Analysis: SEM enables detailed examination of the test specimen's surface by generating high-resolution images. It provides a magnified view of surface features, including wear patterns, scratches, cracks, and other forms of damage that occurred during the tribology test. Additionally, SEM can provide valuable insights into the distribution of elements in the analyzed area.
Wear Mechanism Identification: SEM plays a crucial role in identifying and understanding the wear mechanisms that occurred during the test. By scrutinizing the worn surface at a microscopic level, it becomes possible to determine the types of wear, such as adhesive, abrasive, or fatigue wear. This information is instrumental in diagnosing the underlying causes of wear and developing appropriate solutions.
SEM Procedure To use a Scanning Electron Microscope (SEM) for wear characterization, we followed these steps:

- **Sample preparation**: we prepared the worn sample by pasting it in a specimen holder using a carbon tape.
- **SEM chamber setup**: Ensuring that the SEM is properly calibrated, vacuumed, and ready for operation is important. As for the parameters we used an appropriate acceleration voltage of 15KV, working distance, and spot size based on the sample and desired imaging resolution.
- **Sample loading**: we placed the sample stub carefully into the SEM chamber and secured it in the sample holder, With Making sure that the sample is positioned correctly to ensure the area of interest is in the field of view.
- **Initial imaging**: we started by obtaining an overview image of the worne region using a low magnification to identify the areas of interest and locate the wear features or topographical changes.
- **High-resolution imaging**: Once the areas of interest are identified, we switch to higher magnifications to capture detailed images of the wear features, such as wear tracks, cracks, debris, or surface irregularities.
- **Elemental analysis**: for each specimen, we used an energy-dispersive X-ray spectroscopy (EDS) capabilities of the SEM. which provide us information about the chemical composition of the wear debris or surface layers.

- **Data interpretation**: Analyzing the acquired SEM images to characterize the wear mechanisms, such as abrasive wear, adhesive wear, or fatigue wear.
- **Documentation and reporting**: Capture and save representative SEM images of the wear features.

In conclusion, our experimental procedures encompassed several key steps to comprehensively analyze the thrust pin and insert. We initiated the investigation with chemical analysis, which allowed us to determine the composition of the materials accurately. Subsequently, we conducted a metallographic study to ascertain the steel grade of each component, providing valuable insights into their microstructure. We complemented our analysis by employing scanning electron microscopy (SEM) to investigate the surface characteristics and identify any potential surface treatments.

Moving forward, we delved into the wear behavior of the materials through tribology tests, which allowed us to assess their friction and wear characteristics under controlled conditions. The utilization of a profilometer enabled precise measurements of wear groove depth, contributing to a quantitative evaluation of wear volume and severity, Besides using SEM to verify wear mechanisms observed during the tribology tests. These experimental procedures collectively provided essential insights into the materials' properties, wear behavior, and potential areas for optimization. The knowledge gained from these investigations will serve as a foundation for further analysis and material selection.

Chapter 5

Results and interpretations

Introduction

This chapter provides an overview of the results and interpretation obtained from the characterization of the thrust pin and insert used in this study. The first part encompasses chemical composition analysis, microstructural identification through optical microscope and scanning electron microscope (SEM), surface treatment analysis, as well as hardness and microhardness measurements. These findings will contribute to a better understanding of the properties and behavior of the thrust pin and insert, leading to valuable insights for their application in practical scenarios. While the second part of this study focuses on investigating the wear behavior of the thrust pin and insert through a tribological study. The aim is to understand the intensity of wear and its underlying mechanisms. This analysis involves the use of a profilometer to characterize the wear intensity by measuring wear depth and wear area. Additionally, the scanning electron microscope (SEM) integrated with energy-dispersive X-ray spectroscopy (EDS) technique is employed to further examine the wear mechanisms and identify the elemental composition changes associated with wear. In the third part of this study, we embark on selecting the most appropriate steel for substitution by thoroughly considering multiple crucial factors. Our aim is to provide solid evidence supporting our choice for the optimal steel material to replace the current thrust pin and insert. We assess various mechanical properties, including tensile strength, yield strength, hardness, and toughness, to ensure the selected steel can handle the applied loads and stress conditions efficiently.

5.1 Surface treatment characterizing

5.1.1 Microhardness

In figure 5.1, Vickers micro-hardness measurements were taken at various points moving towards the core of the samples. The results showed that the micro-hardness decreases as we move away from the surface. This decline in micro-hardness provides clear evidence of the presence of a hardened surface in the steel.

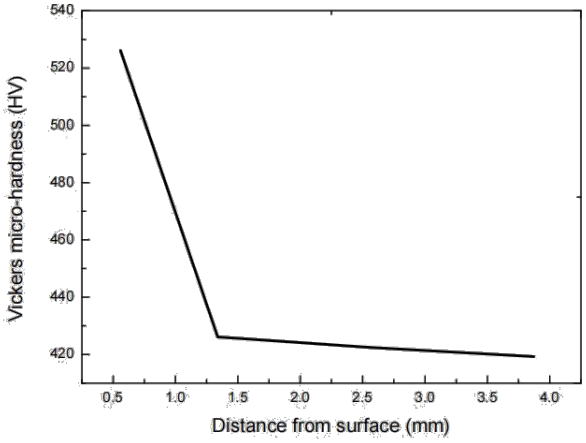

Figure 5.1: Micro-hardness profile

5.1.2 SEM surface treatment characterization

This study focuses on investigating the surface properties of thrust pin and insert that may have undergone specific surface treatments. The objective is to understand the chemical composition and microstructure near the surfaces and correlate these findings with the results obtained from micro-hardness testing. Variations in hardness between the surface and core regions suggest the possibility of localized surface treatments. To support these observations, Scanning Electron Microscopy (SEM) combined with Energy Dispersive X-ray (EDS) analysis is employed for surface analysis. SEM enables high-resolution imaging, providing information about microstructural features, surface morphology, and any surface alterations resulting from treatments or processing. This analysis helps visualize and compare the microstructure near the surfaces and core regions, validating the micro-hardness observations and potentially revealing additional surface characteristics. The integration of EDS analysis with SEM provides a comprehensive understanding of surface chemistry by identifying and quantifying the elemental composition of the material. This information assists in pinpoint-

ing chemical changes resulting from surface treatments.

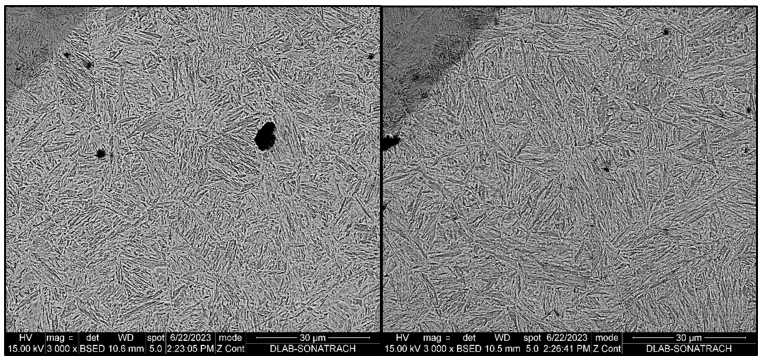

Figure 5.2: SEM micrographs of A) microstructure near indentation of 526.13HV and B) microstructure near indentation of 426.12HV.

From these micrographs, we can't see any specific difference between the microstructures of the region having 526.13HV, and the region having 426.12HV. Both of them appear to be martensitic, except for the presence of pores (default) in different regions of our specimen. Therefore, we conducted a surface elemental analysis to examine the distribution of elements in specific selected areas of both hardness values. Variations in micro-hardness values suggest

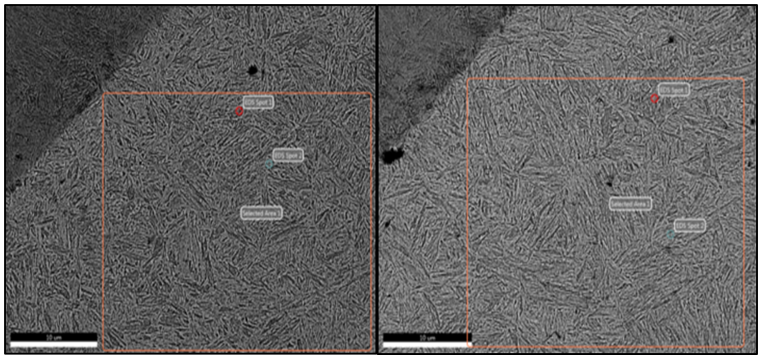

Figure 5.3: SEM micrographs represent selected areas of A) 526.13HV and B) 426.12HV.

the presence of distinct microstructures in these areas. To gain further insights, an Energy Dispersive X-ray (EDX) analysis was conducted to identify and quantify the elemental composition in these regions.

Table 5.1: Micro-hardness area.

Chemical Elements (% Mass)	526.13HV Area	426.12HV Area
Fe	88.67	89.26
C	5.50	5.05
Ni	3.47	3.38
Cr	1.42	1.45
Si	0.93	0.86

The table above presents the mass percentage of elements present in a selected area near the two micro-hardness measurements of 526.13HV and 426.12HV. A notable observation is that the carbon percentage is significantly higher in the area corresponding to the 526.13HV measurement compared to the area associated with 426.12HV. Furthermore, no other elements are detected, supporting the conclusion that the applied surface treatment for the thrust pin and insert is carburizing with a minimum depth of 0.56mm. The higher carbon content in the 526.13HV area indicates a deeper carbon diffusion into the material, indicative of the carburizing process.

5.2 AISI 9310

5.2.1 Chemical composition

We compared the obtained chemical composition with the specifications provided by the American Iron and Steel Institute (AISI) standards. By analyzing the composition of various elements present in the steel samples, starting from the carbon content then focusing on Ni and chromium alloyed steel; and cross-referencing them with the AISI standards, we were able to identify the specific grade of the component accurately.

Table 5.2: Comparison of chemical composition of AISI 9310 and the insert.

Steel	**Content of elements [mass %]**				
	C	**Mn**	**Ni**	**Cr**	**Mo**
Insert	0.1	0.43	3.15	1.29	0.063
AISI 9310	0.08-0.13	0.45-0.65	3.00-3.50	1.00-1.40	0.08-0.15

AISI 9310 is a low alloy steel with nickel, chromium, and molybdenum specifically designed for applications that require high core strength. It possesses a range of desirable properties, including excellent strength, high toughness, good hardenability, and exceptional fatigue strength. In its annealed state, 9310 steel exhibits favorable characteristics such as good ductility, machinability, and cold working properties. Furthermore, it can be easily welded. Due to these advantageous qualities, AISI 9310 steel finds widespread use in various industries, including gear manufacturing, crankshaft production, and heavy-duty applications in the automotive, trucking, and aerospace sectors.

5.2.2 Metallographic study

After conducting research on this steel grade, it was discovered that, according to standard, heat treatment practices typically involve a combination of normalizing, hardening, and tempering as described below:

Normalizing: This is to homogenize the grain structure and enhance machinability. It often involves heating to around 899°C and air cooling.

Hardening: This step aims to increase hardness and strength. It usually involves heating to between 816°C and 871°C, then quenching in oil.

Tempering: This is to reduce brittleness and enhance toughness. It usually involves heating to between 149°C and 371°C, depending on the desired balance between hardness and toughness similarly to as described below.

5.2.2.1 Optical microstructure

The microstructure of AISI 9310 steel after the aforementioned heat treatment process, with a hardness of 36 HRC has likely been tempered to a medium hardness level, resulting in a microstructure that consists of tempered martensite, as observed with an optical microscope using a magnification of X200 and X500 (Figure 5.4).

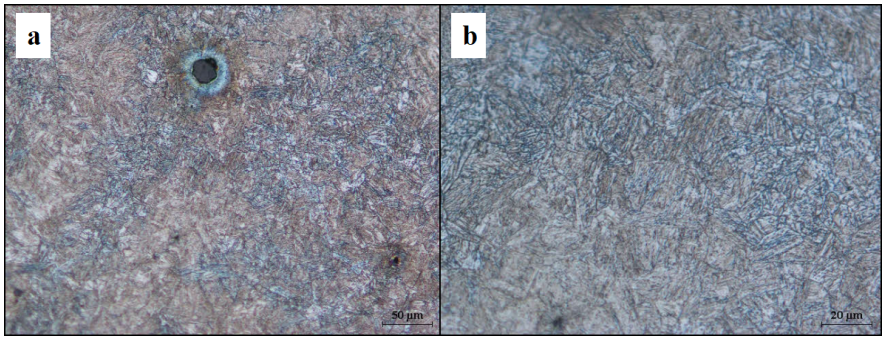

Figure 5.4: Optical micrographs showing microstructure of AISI 9310 at a magnification of a) X200 and b) X500.

Tempered martensite is a microstructure formed when martensitic steel is heated at a temperature where it starts to decompose and form a mixed structure. This typically includes a combination of ferrite (soft and ductile phase) and cementite (hard and brittle phase), or sometimes, a bainitic structure. On a micrograph, tempered martensite appears as fine needle-like structures evenly dispersed in the matrix. Darker areas in the matrix indicates precipitated carbides from the tempering process. Further observation is presented in Figure V.16 using a magnification of X1000 and X1500.

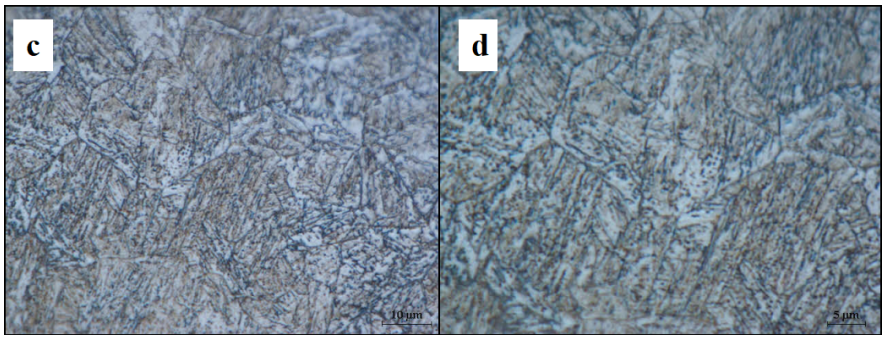

Figure 5.5: Optical micrographs showing microstructure of AISI 9310 at a magnification of c) X1000 and d) X1500.

5.2.3 Mechanical properties

The hardness values obtained for AISI 9310 steel was measured to be 355.23HV (36HRc). The following table presents mechanical properties of AISI 9310.

Table 5.3: Mechanical properties of AISI 9310[1]

Variable	**Yield strength R0.2**	**Tensile strength Rm**	**Elongation at fracture A%**	**Elastic modulus E**	**Rockwell hardness**
Value	900 MPa	1068 MPa	15.50%	200 GPa	36

5.2.4 Wear resistance

The tribological properties of AISI 9310 are crucial in determining its performance and reliability. The experiments conducted using a tribometer, provide valuable insights into the friction and wear characteristics of AISI 9310 under different loading conditions.

5.2.4.1 Friction Force

Friction force measurements were recorded as a function of time for different applied loads ranging from 4N to 12N as illustrated in figure 5.6. We can observe an initial transitional phase of the test, where the friction force increases across all applied loads, due to a higher resistance to motion at the beginning of the test. After a sufficient duration, the curves started to stabilize. This indicates that the contact surfaces reached a steady state where the friction force remained relatively constant. It implies that the steel's response to the applied load had reached an equilibrium state. Notably, the results indicate that applying a load of 4N had a similar effect on the friction force as applying a 6N load. However, a noticeable increase in the friction force was observed for higher loads of 8N, 10N, and 12N. This suggests that the frictional behavior of AISI 9310 steel becomes more pronounced and responsive as the applied load reaches 8N.

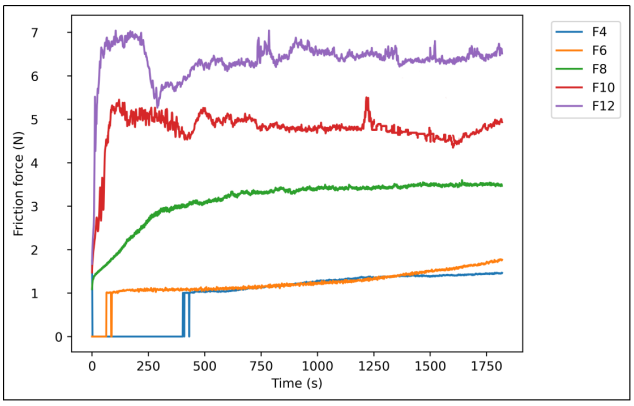

Figure 5.6: Variation of friction force as a function of time for different applied loads.

5.2.4.2 Friction Coefficient

The friction coefficient is a measure of the resistance to sliding motion between two surfaces in contact. It was calculated by dividing the measured friction force by the applied load at each data point. Figure 5.7 indicates variation of the mean value of friction coefficient after a sliding distance of 200 m, in accordance with applied loads. As the applied load increases, the friction coefficient also increases, indicating that surfaces in contact (ball on AISI 9310 sample) experience greater resistance to motion. As the load increases, the contact pressure between the surfaces also increases, leading to a stronger interaction and higher friction coefficient.

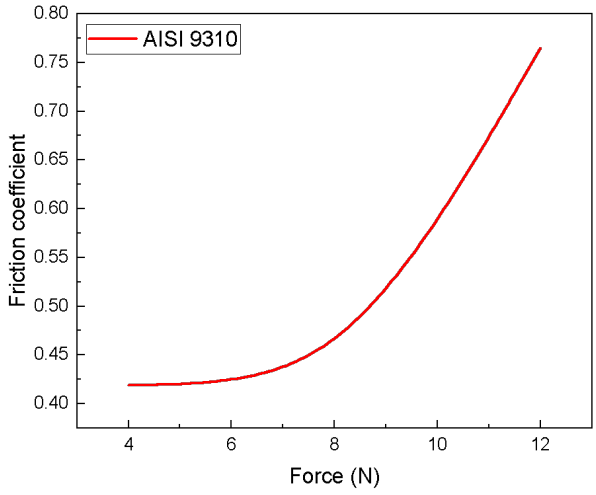

Figure 5.7: Variation of friction coefficient as a function of load applied.

5.2.4.3 Profilometer wear analysis

Similarly, the wear depth and area measurements were also conducted on AISI 9310 under the same conditions to evaluate its behavior. Figure 5.8, comprises two graphs.

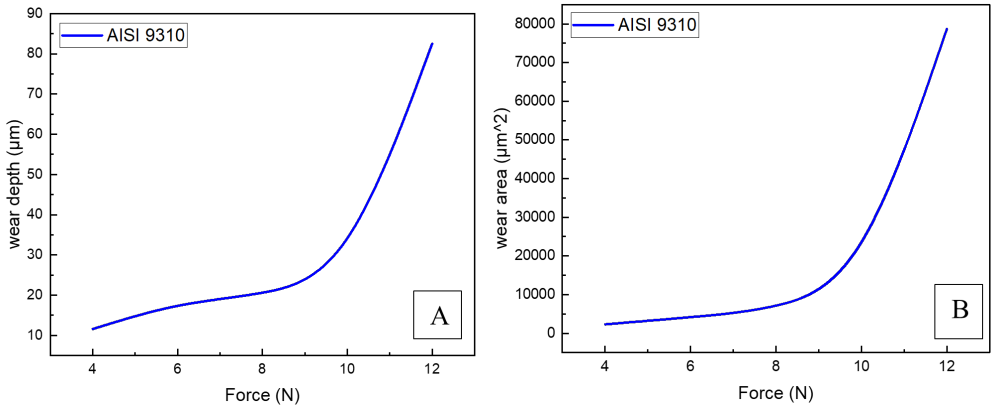

Figure 5.8: Variation of A) Wear depth, and B) wear section according to applied forces on AISI 9310.

The first graph (A) illustrates the wear depth variations, while the second graph (B) represents the changes in wear area for AISI 9310 steel subjected to different applied forces (4, 6, 8, 10, and 12N) after a sliding distance of 200 m. Upon analysis, it is evident that for smaller applied loads (4, 6, 8, and 10N), the wear depth and wear area demonstrate noticeable yet relatively modest variations. However, when the applied force is increased to 12N, a substantial increase in both wear depth and wear area is observed. Specifically, the wear depth reaches a value of 82.5 μm, while the wear area expands to 78721 μm^2. These values significantly surpass the measurements recorded at lower loads, confirming the significant impact of applied force on the wear behavior of AISI 9310 steel.

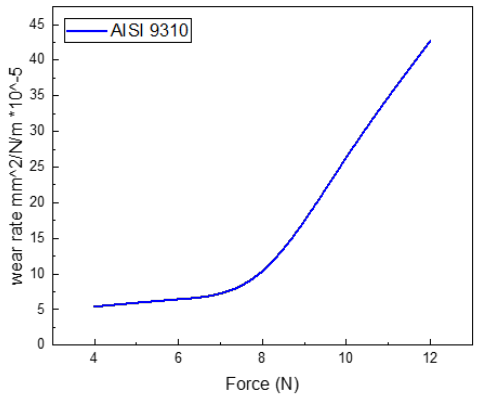

Figure 5.9: Graph of variation of wear rate of AISI 9310 according to different applied load.

Variation of wear rate with respect to the applied load for AISI 9310 steel is illustrated in figure 5.9 after a sliding distance of 200 m. Similar remarkable observations to those observed for wear depth and wear area can be made. For smaller applied loads, the wear rate shows no significant increase, indicating good wear resistance of the material under low forces. However, as the applied load is increased to 12N, the graph clearly demonstrates a substantial rise in wear rate, reaching 42.709x10^{-}5 mm^3/N/m.

5.2.4.4 SEM wear characterizing

A full wear groove micrograph was also captured for AISI 9310 steel to assess the surface damage (Figure 5.10. It is important to note that we used SEM only for the 12N force test. This specific test was chosen because it exhibited a significant increase in wear rate compared to other forces, making it a critical point of analysis. The same technique, namely using an Everhart Thornley Detector (ETD) in secondary electron (SE) mode, was employed to obtain a three-dimensional view. The working distance for this particular micrograph was set at 34.6mm. Upon examination of the micrograph, it is evident that the wear experienced by the AISI 9310 steel is significantly high. Similar to the previous observation, the surface damage is distributed across the wear groove, showcasing a range of different types of damages. Further analysis and description of the specific characteristics of these damages is conducted to gain a more comprehensive understanding of the wear mechanisms involved.

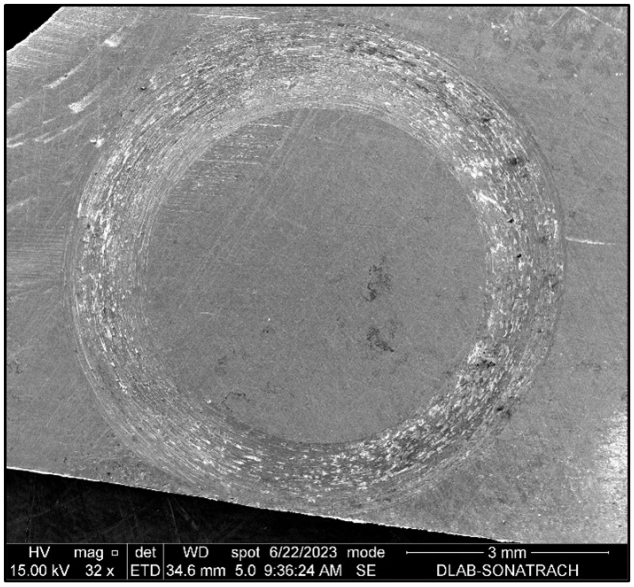

Figure 5.10: SEM micrograph of wear groove morphology of AISI 9310 12N X300.

In Figure 5.11, the SEM micrograph illustrates the worn morphology of the AISI 9310 material after a sliding distance of 200m with a coefficient of friction of 0.530. Similar to the observations made for AISI 9314, the surface of the AISI 9310 material also showcases both smooth and rough patches. The presence of rough patches is noteworthy as they suggest the occurrence of predominant wear. These rough patches indicate areas where significant material removal has taken place. It is likely that the interaction between the sliding surfaces has resulted in localized deformation and damage, leading to the formation of these rough patches.

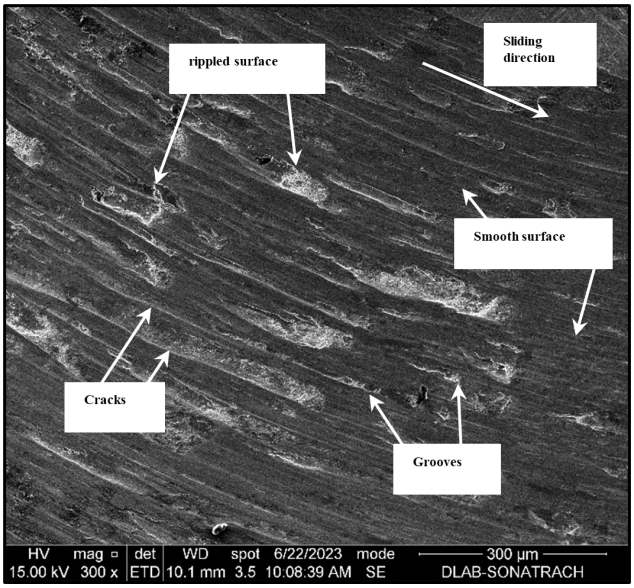

Figure 5.11: SEM micrograph of worn morphology for AISI 9310 steel wear groove with different damages.

The presence of debris is a result of a micro-cutting mechanism that occurs between the connecting surfaces during the sliding process where the surfaces experience shear forces and localized stresses. These forces and stresses can cause the material to undergo micro-cutting, where small fragments of material are sheared off from the surface, detached and then transferred to the surface. The presence of debris indicates the occurrence of additional wear mechanisms in addition to the predominant wear observed in the form of rough patches. The micro-cutting mechanism contributes to the overall wear process and can lead to material removal and surface damage. The presence of debris particles can additionally contrivutrs to abrasive wear by acting as abrasive particles within the sliding surfaces. This further intensifies the wear process [3].

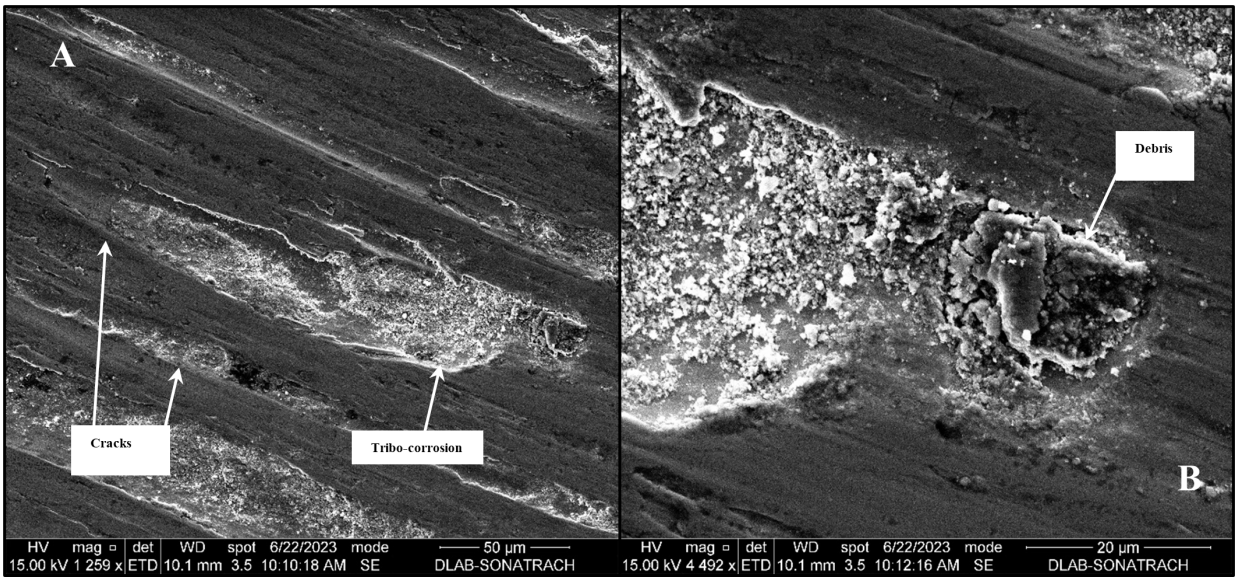

Figure 5.12: SEM micrographs of worn morphology for AISI 9310 steel with a magnification of A) 1259x, and B) 4492x.

In addition to the presence of debris in the AISI 9310 steel, another notable observation is the presence of oxides. These oxides can have implications for a phenomenon called tribo-corrosion. Tribo-corrosion is a combination of mechanical wear and oxidation that occurs when a material is subjected to both sliding or rubbing contact and an oxidating environment. In the case of AISI 9310, the presence of oxides suggests that there might have been simultaneous occurrence of wear and oxidation during the sliding process. During the sliding motion, as the material surfaces come into contact with each other, frictional forces generate heat and can cause localized areas to experience elevated temperatures. These elevated temperatures, combined with the presence of an oxidation environment (humidity in our case), can lead to the formation of oxides on the surface of the material. The presence of these oxides can exacerbate the wear process by acting as abrasive particles, further contributing to material removal and surface damage. Additionally, the oxides may also create localized electrochemical cells, leading to accelerated oxidation in those areas. The occurrence of tribo-corrosion in AISI 9310 steel has implications for the material's durability and performance in applications where both sliding and oxidating conditions are present. To understand their composition and distribution on the material surface, we conducted further investigation and analysis of these oxides to obtain more detailed information about the element distribution. We selected a different surface with a higher occurrence of oxides and performed an EDS analysis. The results, presented in Figure 5.13 and Table 5.4, reveal the findings. It is worth noting that the SEM wear description aligns with the results obtained in previous studies [3,4].

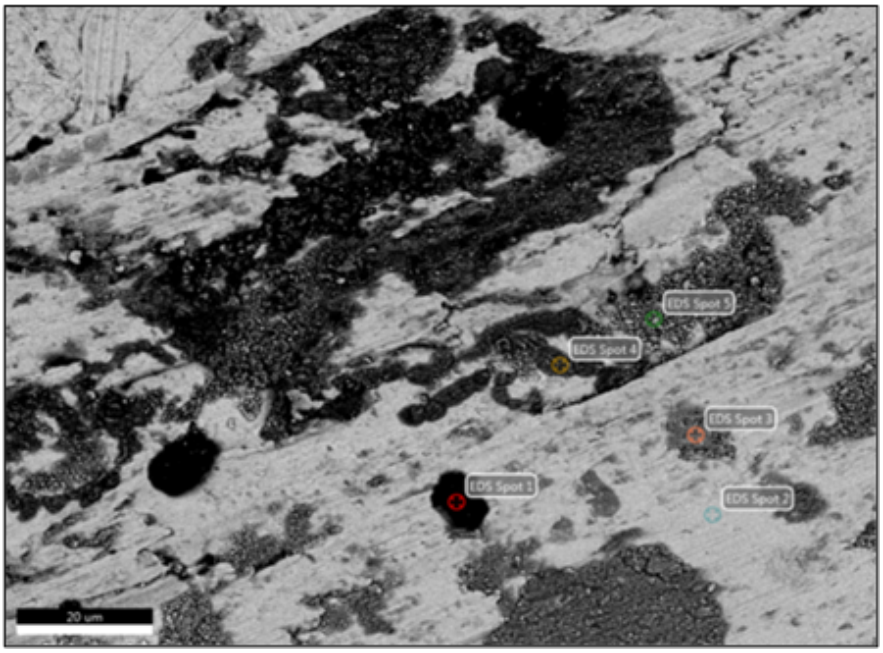

Figure 5.13: SEM micrograph of worn morphology of AISI 9310 with 5 spots X1000.

Table 5.4: Spots with different mass percentage of chemical elements.

		Spot Number				
		1	**2**	**3**	**4**	**5**
Chemical elements [mass%]	**Fe**	48.39	80.52	55.55	46	61.37
	C	30.73	14.48	13.4	15.87	18.39
	Cr	1.4	1.24	1.09	0.89	1.27
	Ni	2.31	2.97	2.2	2.34	2.72
	O	7.22	/	27.04	33.45	15.59
	N	4	/	/	/	/
	Cl	0.76	/	/	0.8	/
	K	0.86	/	/	/	/
	Ca	1.3	/	/	/	/
	Si	0.76	0.78	0.72	0.65	0.66
	Na	1.45	/	/	/	/
	S	0.82	/	/	/	/

Five spots were selected for analysis, representing various regions of the micrograph, ranging from the lightest to the darkest. Spots 1 and 2 were placed in the darkest and lightest areas, respectively. The analysis revealed that the first spot contained mineral salts, with sodium (Na) being the predominant element at a concentration of 1.45%. The presence of these salts may be attributed to moisture deposition around the area. On the other hand, the second spot, located in the lightest area, indicates the absence of oxygen and the presence of self-steel without any signs of oxidation. The remaining three spots (3, 4, and 5) were chosen from spotted gray regions contain debris. The table shows that all three spots exhibited the presence of oxygen with varying percentages. This confirms the presence of oxides within the debris. Spot number 4 exhibited the highest percentage of oxygen among the three spots, indicating a higher concentration of oxides in that region. This finding supports the hypothesis that this specific spot or area is associated with the presence of oxides. The presence of these oxides in the debris suggests the occurrence of tribo-corrosion, a phenomenon commonly observed in low-alloy steel. These results align with previous studies [3,4] that reported similar SEM wear descriptions.

5.3 AISI 9314

5.3.1 Chemical composition

AISI 9314 is a nickel-chromium-molybdenum case-hardening steel known for its high strength, toughness, and hardenability. It is commonly used in applications requiring robust performance, such as gears, crankshafts, and heavy-duty machinery components. With its excellent combination of strength, toughness, and machinability, AISI 9314 steel is suitable for demanding industries like automotive and aerospace. Weldability and the ability to achieve desired properties through heat treatment further enhance its versatility.

Table 5.5: Comparison of chemical composition of AISI 9314 and the pin.

Steel	**Content of elements [mass %]**				
	C	**Mn**	**Ni**	**Cr**	**Mo**
Pin	0.13	0.45	3.35	1.28	0.064
AISI 9314	0.11-0.17	0.40-0.70	3.00-3.50	1.00-1.40	0.08-0.15

5.3.2 Metallographic study

AISI 9314 is a nickel-chromium-molybdenum case-hardening steel alloy that can be heat-treated to increase its hardness and strength. It involves the following steps:
Normalizing: This involves heating the steel to a temperature above its critical point, around 870-910°C, and then allowing it to cool in open air. This helps to homogenize the alloy and prepare it for further heat treatments.
Quenching: After carburizing, the steel is quickly cooled by immersing it in oil or water. This rapid cooling hardens the steel by causing it to form a martensitic structure.
Tempering: After quenching, the steel is still very brittle, so it's heated to a lower temperature (around 200°C) to relieve stresses and increase toughness.

5.3.2.1 Optical microstructure characterizing

For AISI 9314 steel with a hardness of 41 HRC, the microstructure obtained is tempered martensite. This is because the hardness of the steel indicates the steel has been tempered to a medium hardness level. This specific microstructure could be observed with an optical microscope using the magnification of X 200 and X500 (Figure 5.14).

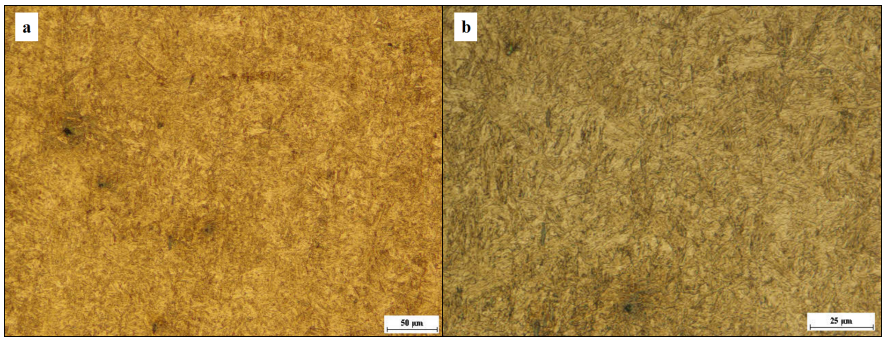

Figure 5.14: Optical micrographs showing microstructure of AISI 9314 at a magnification of a) X200 and b) X500.

This microstructure appears as dark needle-like shapes (martensite) distributed in a lighter matrix (ferrite and cementite). Carbides are also visible. Detailed observation of needle-like shapes and carbides could be obtained using a magnification of X1000 and X1500.

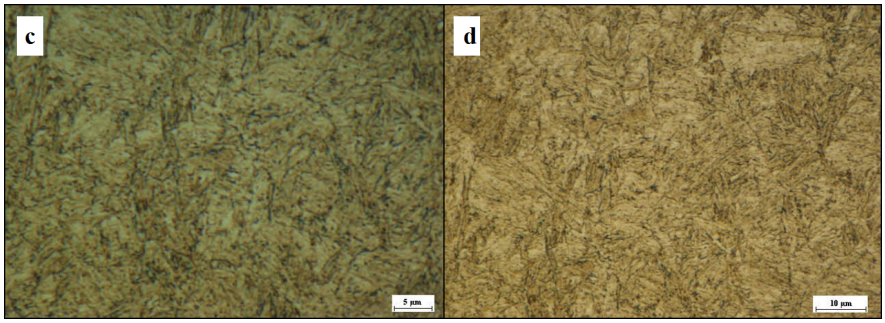

Figure 5.15: Optical micrographs showing microstructure of AISI 9314 at a magnification of c) X1000 and d) X1500.

5.3.2.2 SEM Microstructure characterizing

After confirming the microstructure using an optical microscopy, it is optional but beneficial to utilize scanning electron microscopy (SEM) for further microstructural identification. SEM provides higher magnification and detailed imaging, allowing us to observe the microstructure at a much finer scale. This additional level of analysis can help confirm the microstructural features identified through optical microscopy and provide more comprehensive insights into the material's internal structure. We decided to use scanning electron microscopy (SEM), specifically for AISI 9314, to confirm the results. The SEM micrograph obtained is shown in the following figure:

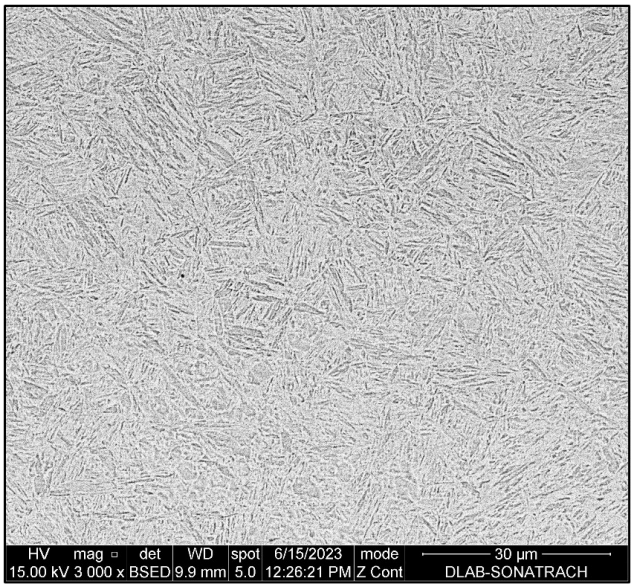

Figure 5.16: SEM micrograph of AISI 9314 microstructure under a magnification of 3000X.

The figure above is an SEM micrograph for AISI 9314 taken with a BSED detector using a Z cont mode from a working distance of 9.9 mm. it represents and confirm the microstructure obtained by the optical microscope which is tempered martensitic. By confirming the microstructural features through SEM imaging, we can strengthen our understanding of the material's internal structure and gain more confidence in the results obtained from optical microscopy. This combined approach of using both microscopy techniques enhance the reliability of our microstructural analysis, contributing to a more comprehensive assessment of AISI 9314 steel's properties and behavior.

5.3.3 Mechanical properties

The hardness values obtained for AISI 9314 steel was measured to be 400.15HV in average (41 HRc) .Table—presents mechanical properties of AISI 9314.

Table 5.6: Mechanical properties of AISI 9314 [2].

Variable	**Yield strength R0.2**	**Tensile strength Rm**	**Elongation at fracture A%**	**Elastic modulus E**	**Rockwell hardness**
Value	1034 MPa	1158 MPa	15%	190-210 GPa	41

5.3.4 Wear resistance

The importance of understanding the tribological behavior of AISI 9314 is paramount in ensuring efficient and reliable performance in engineering applications. AISI 9314, a widely used steel alloy, exhibits excellent mechanical properties. The main objective of this study is to investigate the friction and wear behavior of this steel grade and analyze the variation of friction coefficient and friction force under different applied loads.

5.3.4.1 Friction force

The measured friction force as a function of time was recorded for each load ranging from 4N to 12N as illustrated in figure 5.17, we can observe an initial transitional phase of the test, where the friction force increases across all applied loads. After a certain duration that increases with the load applied, the curves stabilize.

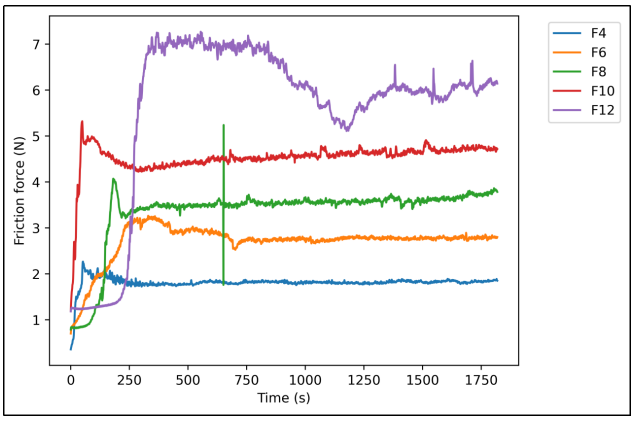

Figure 5.17: Variation of friction force as a function of time for different loads applied.

5.3.4.2 Friction coefficient

Based on the tribometer test conducted on AISI 9314 with different loads (4N, 6N, 8N, 10N, and 12N). Figure 5.18 represents the mean value of friction coefficient after a sliding distance of 200 m, in accordance with loads applied. From the graph above, it is evident that there is a trend of increasing friction coefficient with increasing load, especially beyond 10N. This behavior indicates that with higher loads, the contact area between AISI 9314 steel material and the mating surface may increase. A larger contact area can increase the adhesion and frictional forces between the surfaces, resulting in an increased friction coefficient.

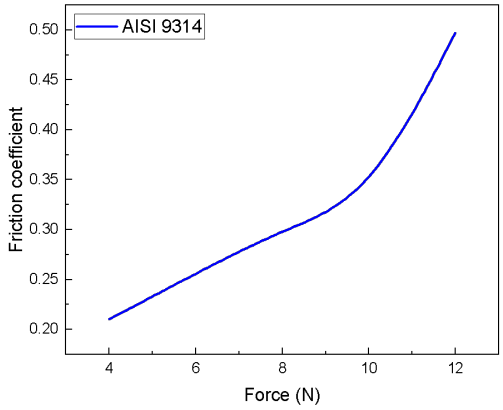

Figure 5.18: Variation of friction coefficient as a function of load applied.

5.3.4.3 Profilometer wear analysis

After conducting profilometer measurements on the surface, the system analyzes the data to determine the wear area, wear depth and more importantly wear rate. In order to investigate the wear characteristics of the material under different loading conditions, we intentionally varied the load during the testing process. The figure 5.19, showcases two graphs.

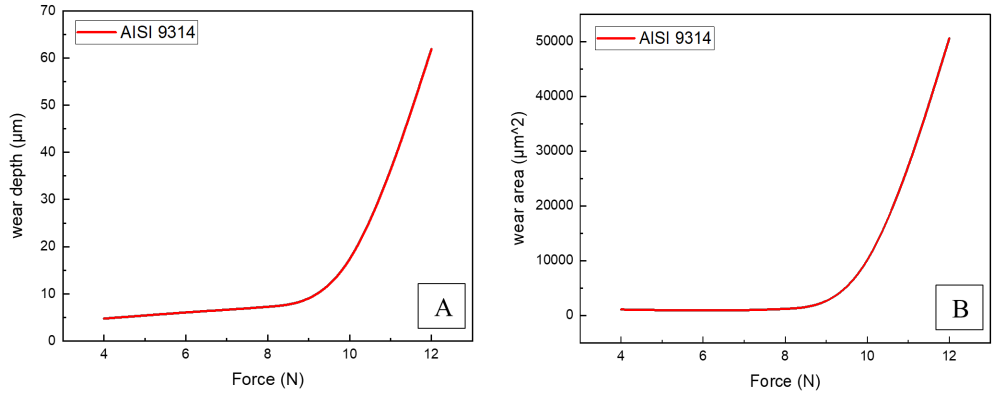

Figure 5.19: Variation of A) Wear depth, and B) wear section according to applied forces on AISI 9314.

The first graph (A) illustrates the variations in wear depth, while the second graph (B) depicts the changes in wear area for AISI 9314 steel under different applied forces (4, 6, 8, 10, and 12N) after a sliding distance of 200 m. Notably, the results reveal that for smaller loads (4, 6, 8, and 10N), there is only a slight progression in the wear depth and area. However, when the load is increased to 12N, a significant increase in both wear depth and area occurs. The wear depth reaches a value of 61.9 μm, while the wear area expands to 50582 μm^2. These values are considerably higher compared to the measurements observed at lower loads. This observation emphasizes the substantial influence of applied force on the wear behavior of AISI 9314 steel.

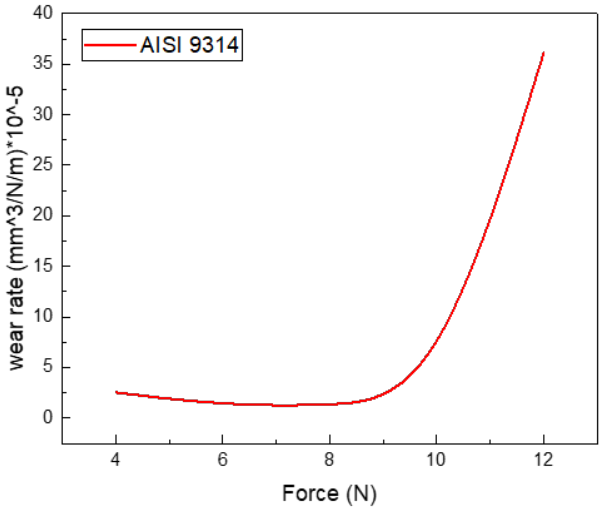

Figure 5.20: Graphs of variation of wear rate of AISI 9314 according to different applied load.

Variation of the wear rate according to applied load after a sliding distance of 200 m is presented i figure 5.20. The same remarkable observations of wear depth and wear section apply to the wear rate. For small loads, there is no progressive increase in wear rate, indicating good wear resistance of this material against small forces. However, when the applied load increases to 12N, we can confirm from the graph that the wear rate increases to $36.121 \times 10^{-}5$ $mm^3/N/m$.

5.3.4.4 SEM wear characterizing

The SEM analysis was used to examine the worn path of AISI 9314 steel in order to recognize the wear mechanism better. The full wear groove was captured to obtain an overall understanding of the surface damaged from a working distance of 26.3mm.(Figure 5.21). The micrograph clearly reveals that the wear experienced by the material was significantly pronounced. The surface damage is distributed throughout the wear groove and exhibits various types of damage. The specific details of the various types of damage and their characteristics can be further analyzed and described for a more comprehensive understanding. In Figure 5.22, the scanning electron microscopy (SEM) micrograph displays the worn morphology of the AISI 9314 steel after a sliding distance of 200m resulting in a friction coefficient of f=0.528.

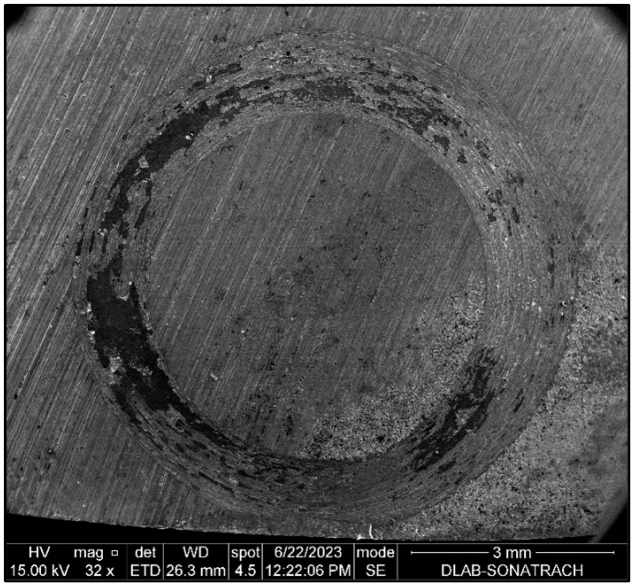

Figure 5.21: SEM micrograph of Worn morphology of AISI 9314 wear groove 12N.

The surface of the material exhibits both smooth and rough patches. The rough patches are particularly interesting as they indicate predominant wear. Within the rough patches, a rippled surface is visible. This rippled surface is a clear indication of wear and suggests that significant material removal has occurred. The formation of these ripples is likely due to the interaction between the sliding surfaces, resulting in localized deformation and damage. Additionally, (Figure 5.22 A)shows the presence of a crater on the material surface. This crater is formed as a result of the sliding action and represents a localized area of material removal. It is noteworthy that no debris is shown within the crater, suggesting that any loose particles or wear debris generated during the sliding process have been transported away from the area by subsequent cycles. The shape and characteristics of the crater provide valuable insights into the wear mechanism that took place. The presence of cracks in the surrounding region of the crater suggests that surface dislocations and damage occurred during the sliding process. These cracks may have been initiated and propagated due to the stress and strain imposed on the material as a result of sliding contact. In summary, (Figure 5.22) A and B depict the worn surface of the AISI 9314 steel after sliding for a distance of 200m. The presence of smooth and rough patches, along with a rippled surface and a crater, indicates significant wear and localized material removal. The observations provide clues about the wear mechanisms involved which is micro-cutting, including surface dislocations, damage, and the potential for crack formation, this SEM wear discreption similar to results obtained by [3].

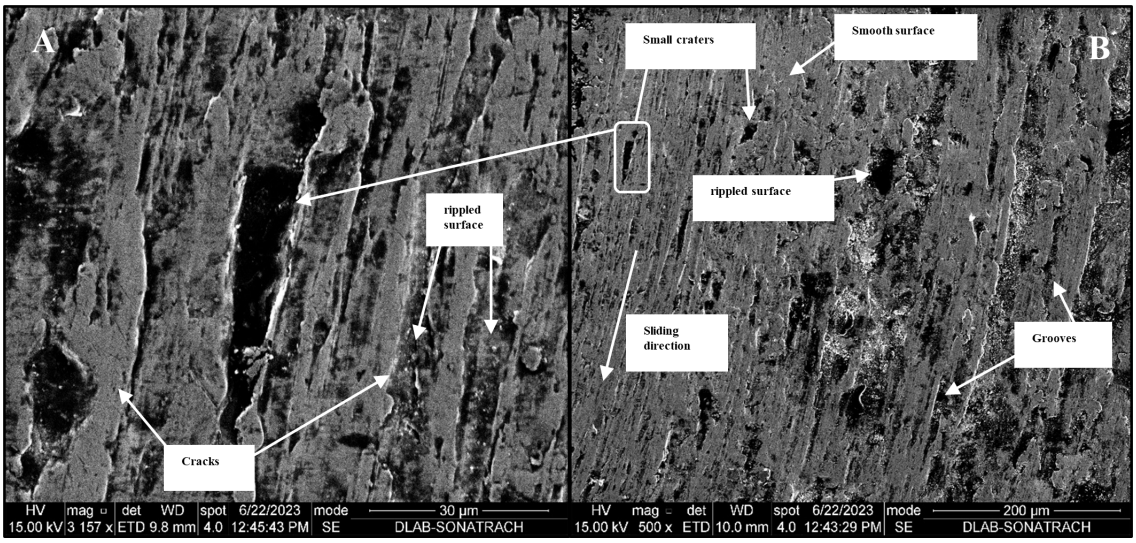

Figure 5.22: SEM micrograph Worn morphology of AISI 9314 with different magnifications and damages A) 3157x, B) 500x.

5.4 Introducing steel grade selection

The selection of a substitute steel involves careful consideration of specific factors to ensure that the chosen material meets the desired requirements and performs effectively during drilling operations. In our case, the aim was to find a suitable substitute steel that would offer improved hardness, possess a chemical composition similar to AISI 9310 and AISI 9314, exhibit enhanced wear resistance, with the inclusion of molybdenum (Mo) in the substitute steel. Additionally, since the insert component, which was originally manufactured with AISI 9310, is subjected to shocks and susceptible to damage more than the pin, the primary objective was to find a substitute steel grade with a hardness exceeding 36 HRc. After extensive research among numerous steel grades that satisfied these desired characteristics, the steel grade chosen as the optimal substitute was AISI 4337. Reasons we took into consideration are explained below:

Improved Hardness: By seeking a substitute steel with better hardness characteristics, the goal is to enhance the material's durability and longevity under load, resulting in improved performance and reduced maintenance requirements.

Similar Chemical Composition: Choosing a substitute steel with a chemical composition close to AISI 9310 and AISI 9314 is advantageous as it allows for compatibility in terms of metallurgical properties, such as heat treatment and weldability.

Enhanced Wear Resistance: By selecting a substitute steel with superior wear resistance, it becomes possible to mitigate surface damage, extend the system (pin-insert) lifespan, and reduce the frequency of replacements. This leads to cost savings and improved overall performance in demanding operational environments.

Inclusion of Molybdenum (Mo): Molybdenum is an alloying element that offers several beneficial properties to steel. It can contribute to improved strength, toughness, and resistance to wear and corrosion. The presence of molybdenum in the substitute steel enhances its overall performance and provides advantages over other materials that lack this element.

5.5 AISI 4337

5.5.1 Chemical composition

AISI 4337 is a high-strength, low-alloy (HSLA) steel that is primarily used in the aerospace and automotive industries. It is a French steel grade that conforms to the European standard EN 10025-6. AISI 4337 is known for its excellent mechanical properties and toughness, making it suitable for applications that require high strength and resistance to impact and fatigue. The steel's composition, including elements such as chromium and molybdenum, contributes to its wear resistance. This makes it suitable for parts subjected to sliding, abrasion, or contact with other surfaces. Chemical composition of this steel grade is presented in the following table.

Table 5.7: Chemical composition of AISI 4337 steel.

Steel	**Content of elements [mass %]**									
	C	**Mn**	**Ni**	**Cr**	**Mo**	**V**	**Cu**	**Si**	**S**	**P**
AISI 4337	0.35	0.56	3.4	0.83	0.16	0.03	0.26	0.29	0.013	0.032

5.5.2 Metallographic study

5.5.2.1 Optical microstructure characterizing

The microstructure of AISI 4337 steel was observed with an optical microscope using magnifications of X200, X500, and X1000 as shown in figure V. Having a hardness of 39 HRC, the resulting microstructure consistes of tempered martensite. On the micrographs, tempered martensite appears as fine needle-like structures evenly dispersed in the matrix. Darker areas in the matrix indicates precipitated carbides from the tempering process that helps in enhancing the steel's strength and wear resistance. Further observation is presented in Figure 5.24 using a magnification of X1000.

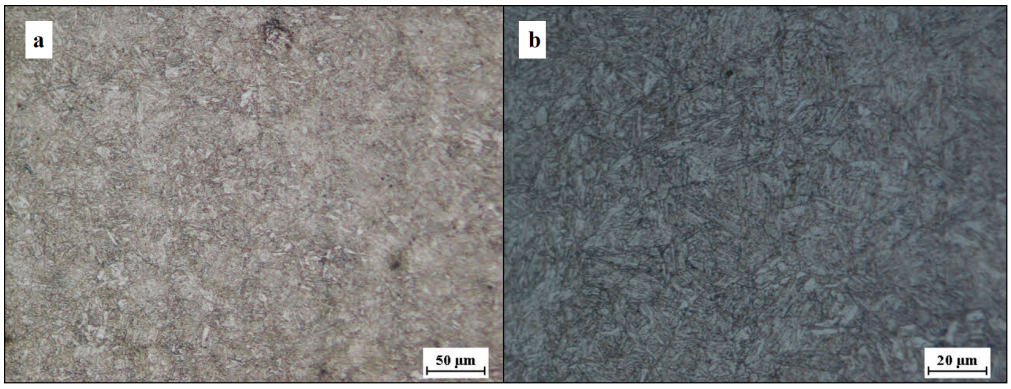

Figure 5.23: Optical micrographs showing microstructure of AISI 4337 steel at a magnification of a) X200 and b) X500.

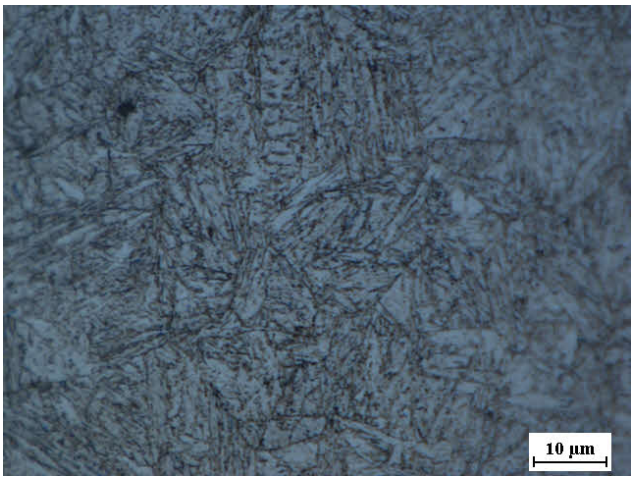

Figure 5.24: Optical micrographs showing microstructure of AISI 4337 steel at a magnification of X1000.

5.5.3 Mechanical properties

The heat treatment process outlined in chapter 04, involves austenitizing the steel at a temperature of 880 °C for a duration of 40 minutes, followed by quenching and tempering at 550 °C for one hour. As a result of this heat treatment, the steel attains a hardness value of 39HRc.

Table 5.8: Mechanical properties of AISI 4337.

Variable	**Yield strength R0.2**	**Tensile strength Rm**	**Elongation at fracture A%**	**Elastic modulus E**	**Rockwell hardness**
Value	740 MPa	850 MPa	15%	157 GPa	39

5.5.4 Wear resistance

The tribological properties of AISI 4337 steel are crucial in determining its performance and reliability to substitute the components that's showing little wear resistant.

5.5.4.1 Friction Force

Figure 5.25 illustrates the recorded measurements of friction force as a function of time, with applied loads ranging from 4N to 10N. Similar to steels AISI 9310 and AISI 9314, we can observe an initial transitional phase in the test, during which the friction force increases across all applied loads. However, this increase quickly stabilizes, indicating that the steel has reached an equilibrium state in response to the applied load.

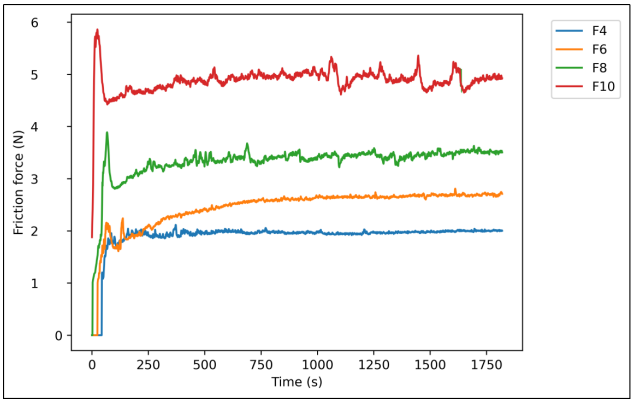

Figure 5.25: Variation of friction force as a function of time for different applied loads on AISI 4337.

5.5.4.2 Friction Coefficient

In Figure 5.26, the mean value of the friction coefficient is shown as it varies with different applied loads after a sliding distance of 200 m, specifically in the context of the ball sliding on a AISI 4337 steel sample. The results demonstrate that as the applied load increases, the friction coefficient also increases. This observation suggests that the surfaces in contact experience greater resistance to motion. The increase in friction coefficient with higher applied loads is attributed to the increased contact pressure between the surfaces. As the load increases, the pressure between the ball and the AISI 4337 steel sample intensifies. This heightened pressure leads to a stronger interaction between the surfaces, resulting in a higher friction coefficient.

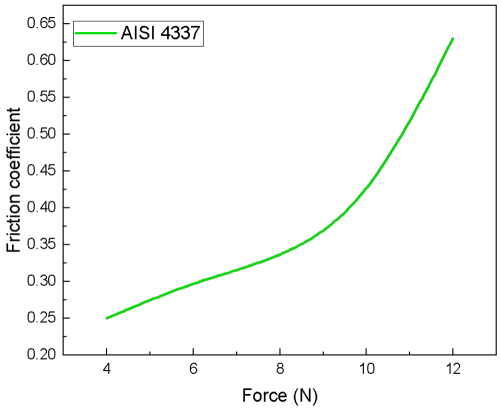

Figure 5.26: Variation of friction coefficient as a function of loads applied on AISI 4337 steel.

5.5.4.3 Profilometer wear analysis

The same tribology test in the same condition provided for AISI 4337 where we varied load from 4N to 12N to analyze wear behavior of this steel. The following figure represents wear depth and wear section according to applied load after a sliding distance of 200 m.

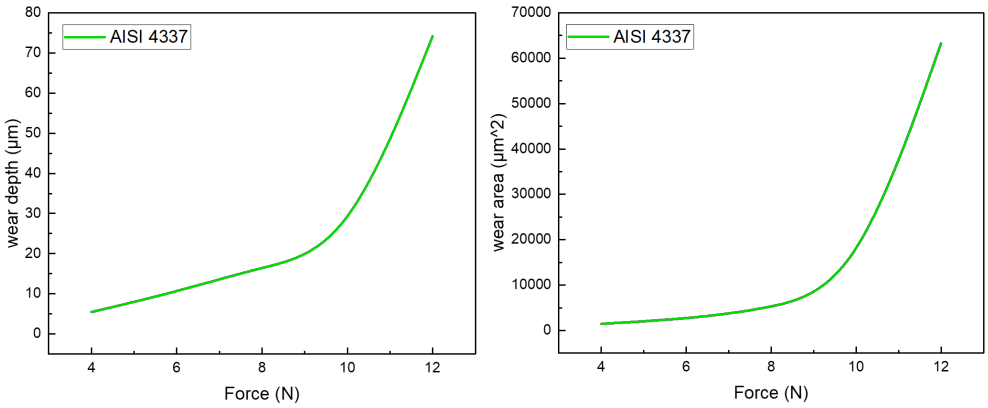

Figure 5.27: Variation of A) Wear depth, and B) wear section according to applied forces on AISI 4337.

The above Figure consists of two graphs (A and B) illustrating wear characteristics of AISI 4337 steel under different applied forces (4, 6, 8, 10, and 12N) after a sliding distance of 200 m. Upon analysis, it becomes evident that for smaller applied loads (4, 6, 8N), both wear depth and wear area exhibit noticeable yet relatively modest variations. However, as the applied force increases to 12N, a significant escalation in both wear depth and wear area is observed. Specifically, the wear depth reaches a value of 72.2 μm, and the wear area expands to 63258 μm^2. These values substantially exceed the measurements recorded at lower loads, emphasizing the substantial influence of applied force on the wear behavior of AISI 4337 steel.

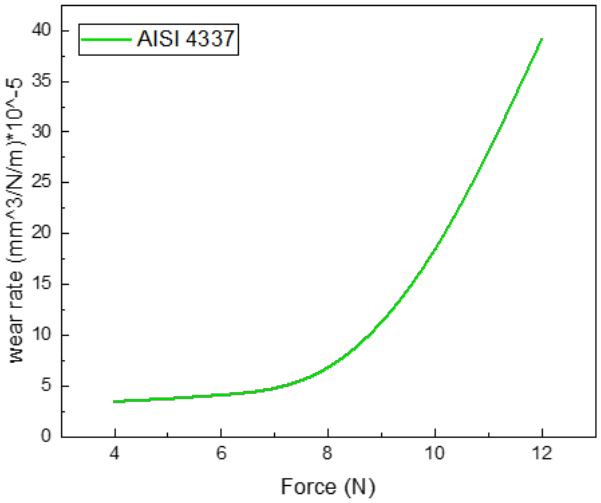

Figure 5.28: Graph of variation of wear rate of AISI 4337 according to different applied load.

Figure 5.28 presents the variation of wear rate in AISI 4337 steel with respect to the applied load after a sliding distance of 200 m. Similar to the observations made for wear depth and wear area, distinct trends can be noted in the wear rate. For smaller applied loads, the wear rate shows no significant increase, indicating that the material exhibits good wear resistance under low forces. This is a favorable characteristic as it implies that AISI 4337 steel can withstand wear and abrasion effectively under lighter loads. However, as the applied load is increased to 12N, the graph clearly depicts a substantial rise in wear rate. The wear rate reaches a value of $39.16 \times 10^{-}5$ $mm^3/N/m$., signifying a considerable increase in material removal under higher forces. This finding emphasizes the sensitivity of wear behavior in AISI 4337 steel to varying applied loads, indicating that the material may experience accelerated wear and deterioration when subjected to higher forces.

5.5.4.4 SEM wear characterizing

For the proposed steel, we also provided an SEM characterizing the wear groove with the same condition as AISI 9314 and AISI 9310.

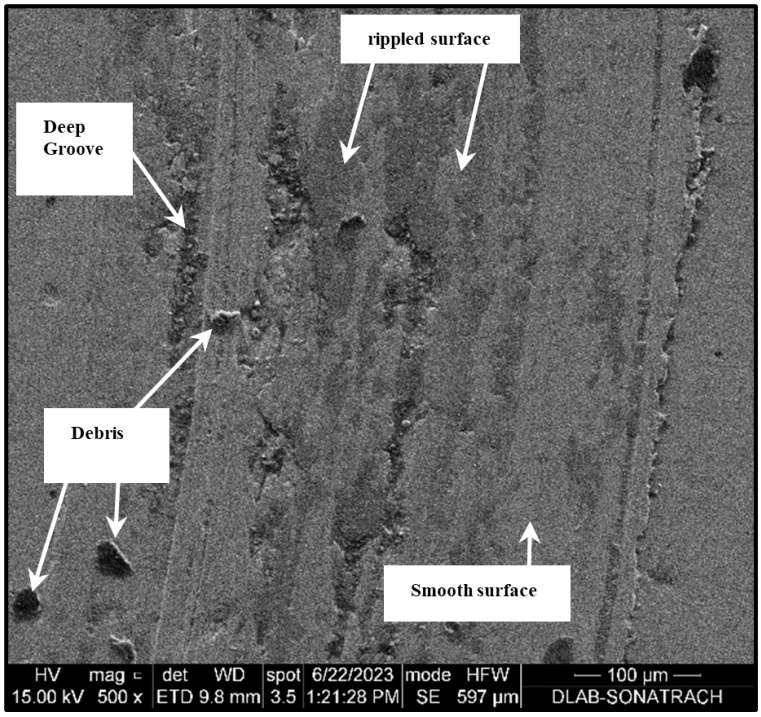

Figure 5.29: SEM micrograph of Worn morphology of AISI 4337 wear groove 12N.

The figure 5.29 above illustrates the worn morphology of the AISI 4337 material after a sliding distance of 200 m and a friction coefficient of 0.63. the damage is quite similar to AISI 9314 and AISI 9310 steels, however the wear groove width is smaller than AISI 9310. The presence of noticeable rough patches in the surface analysis is significant, as they strongly indicate the occurrence of predominant wear. These rough patches are clear evidence of substantial material removal, suggesting that the sliding surfaces have experienced significant interaction and localized deformation during the wear process. The abrasive action between the surfaces has likely caused damage and deformation, resulting in the formation of these rough patches. The figure below is an SEM micrograph, magnified at 3157x, showcasing the damage that occurred after a sliding distance of 200 m. In this micrograph, a distinct crater is visible. AISI 4337 steel presents fewer and smaller debris. This reduction in debris indicates less damage, as these debris particles often act as a third body during sliding, accelerating wear and making it more pronounced. The observation of reduced debris in AISI 4337 steel suggests that it exhibits better wear resistance and durability compared to AISI 9310. The presence of fewer debris particles indicates that the wear process in AISI 4337 is less severe and results in a lower rate of material removal.

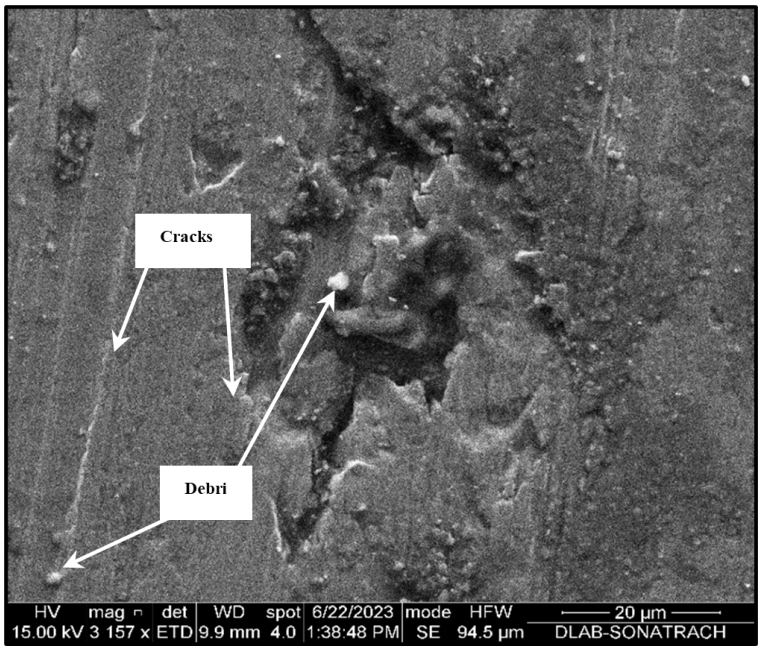

Figure 5.30: SEM micrograph Worn morphology of AISI 4337 presenting a crater with 3157X magnifications.

5.6 Comparison study between AISI 9314, AISI 9310, and AISI 4337 steels

5.6.1 Friction coefficient

The friction coefficients of AISI 9310, AISI 9314, and AISI 4337 exhibit an increasing trend as the applied load varies from 4N to 12N. Among these steel grades, AISI 9314 demonstrates the lowest friction coefficient values, a maximum of 0.45 indicating its superior resistance to frictional forces. Following AISI 9314, the friction coefficients for AISI 4337 are slightly higher, a maximum of 0.63, but still lower compared to AISI 9310 (0.77 maximum), which exhibits the highest friction coefficients within this group. AISI 9314 exhibits the best resistance to friction among the steel grades tested (AISI 9310, AISI 9314, and AISI 4337) when subjected to loads ranging from 4N to 12N. It has the lowest friction coefficient values, indicating reduced friction between contacting surfaces. AISI 4337 performs as the second-best, displaying better frictional characteristics than AISI 9310 despite slightly higher friction coefficients. AISI 9310 shows the highest friction coefficients, indicating lower resistance and higher frictional forces compared to AISI 9314 and AISI 4337 within the specified load range.

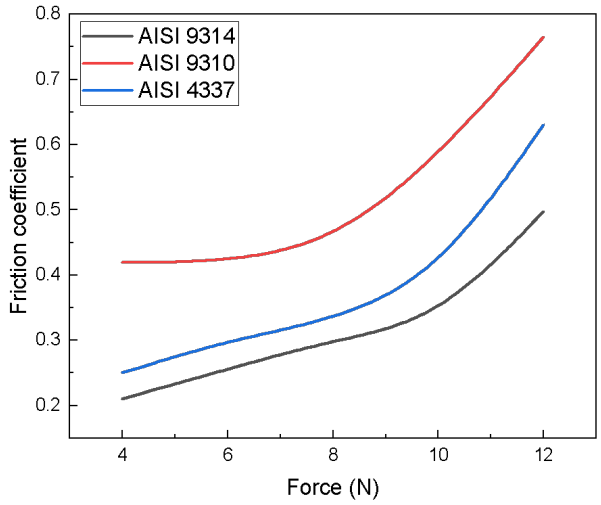

Figure 5.31: Comparison between the friction coefficient of the three steel grades.

5.6.2 Wear rate

Figure 5.32presents a comparison of wear rate between AISI 9314, AISI 9310 and AISI 4337 after a wear test under the same conditions of sliding. It is clear that:

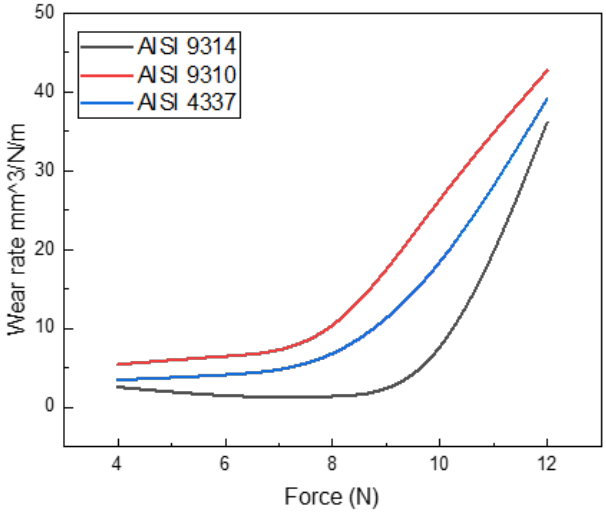

Figure 5.32: Comparison Graph between AISI 9314, AISI 9310 and AISI 4337 about variation of wear rate according to different applied load.

- Small to no variation of wear rate for 4, 6, 8N for all of the steel grades.
- Wear rate of AISI 9310 for different loads is more than AISI 9314.
- AISI 9314 is more resistant than AISI 9310 and AISI 4337.
- Resistance of AISI 4337 is intermediate between AISI 9314 and AISI 9310.

5.6.3 Wear morphology

Comparing the previous results, we found that:

- The micrographs of AISI 9314 and AISI 9310 steel after a sliding distance of 200m reveal significant wear and surface damage distributed across the wear groove. Various types of damage, including rough patches and ripples, indicate localized deformation and material removal.
- Both AISI 9314 and AISI 9310 steels exhibit rough patches, suggesting predominant wear and significant material removal. However, AISI 9310 shows more debris, indicating a micro-cutting mechanism during sliding and potential tribo-oxidation due to the presence of oxides.
- The observation of reduced debris in AISI 4337 steel suggests that it exhibits better wear resistance and durability compared to AISI 9310. The presence of fewer debris particles indicates that the wear process in AISI 4337 is less severe and results in a lower rate of material removal.
- The SEM analysis of the proposed steel (AISI 4337) under similar conditions as AISI 9314 and AISI 9310 steels reveals comparable damage. however, AISI 4337 steel exhibits fewer and smaller debris particles, indicating better wear resistance and reduced material removal compared to AISI 9310 steel.

5.7 Global interpretation

- AISI 9314 has higher carbon content and hardness than AISI 9310, making it inherently harder.
- The higher hardness of AISI 9314 contributes to its enhanced wear resistance.
- AISI 9314 exhibits a lower wear rate, indicating superior resistance to wear compared to AISI 9310.
- AISI 4337 shows greater wear resistance than AISI 9310, attributed to its higher carbon content and molybdenum presence.
- AISI 4337's wear resistance is enhanced by its higher molybdenum content.
- AISI 9314 outperforms AISI 4337 in wear resistance despite having lower percentages of elements for hardness.
- Heat treatment likely played a crucial role in achieving AISI 9314's wear resistance.
- The wear resistance of AISI 4337 and AISI 9314 is influenced by their respective chemical compositions and hardness levels.
- AISI 4337 is selected as a suitable substitute for AISI 9310 based on its wear resistance and optimized performance for thrust pin and insert system.

Conclusion

In conclusion, our research on the characterization and wear resistance analysis of thrust pins and inserts in high-speed drilling motors has yielded significant insights and contributions to the field of materials engineering in the oil and gas industry.

Through our comprehensive investigation, we have successfully achieved the objectives of understanding the wear behavior of different steel grades, evaluating the effectiveness of steel grade substitution, and optimizing the performance of thrust pins and inserts.

Our findings have demonstrated that wear resistance is a critical factor in the selection of materials for drilling components. We have identified key wear mechanisms and factors influencing wear performance, providing valuable knowledge for materials engineers in their decision-making processes.

By exploring metallography and heat treatments of structural steel, we have gained a deeper understanding of the microstructural properties and the influence of heat treatment processes on wear resistance. This knowledge has enabled us to recommend suitable steel grade substitutions that enhance the wear resistance of thrust pins and inserts, ultimately increasing their life cycle and reducing maintenance costs.

The implications of our research are far-reaching for the oil and gas industry. By optimizing the wear resistance of thrust pins and inserts, drilling operations can experience improved operational efficiency, reduced downtime, and increased productivity. The economic benefits are significant, as minimized maintenance costs and increased component lifespan contribute to enhanced profitability and competitiveness.

To further sharpen this study, there are several perspectives to consider:

- Long-term wear testing under realistic operating conditions can provide insights into the actual lifetime of these components.
- Developing wear models and simulations can predict the lifetime based on wear mechanisms, drilling parameters, and material properties.
- Advanced material characterization techniques, such as in-situ microscopy and surface analysis, can identify critical wear parameters and failure modes.
- Integrating wear resistance considerations into component design can optimize wear performance and enhance durability.
- Continuously exploring and developing novel steel alloys with enhanced wear resistance properties can improve component lifetimes.

References

References

Chapter 01

[1]. Blake Flournoy. "Oil Drilling Benefits". [Online]. [Visited on 23/04/2018].

[2]. REBECCA MCCLAY. "How the Oil and Gas Industry Works". [Online]. [Visited on 08/06/2023].

[3]. BC Oil and Gas Commission. "Oil and Gas wells: Drilling activity", British Columbia, March 2019.

[4]. Drilling Industry Glossary. [Online]. [Visited on 02/06/2023].

[5]. Esraa Ismail, MOHD AAMIR. "ADNOC leverages advanced technologies to enhance drilling efficiencies". [Online]. [Visited on 15/06/2023].

[6]. BearingNews. "Rack and Pinion Jacking System Bearings on Jack-up rigs". [Online]. [Visited on 15/06/2023].

[7]. Fabio Palmigiani. "Petrobras sticks to a streamlined drilling plan with a reduced fleet". [Online]. [Visited on 14/06/2017].

[8]. Sharda. Marine Insight. "Semi-Submersible Ships and Semi-Submersible Rigs: A General Overview". [Online]. [Visited on 14/06/2023].

[9]. Norwell edge. "Introduction to drilling", Massachusetts, October 2019. [Online]. [Visited on 15/06/2023].

[10]. Dragon. "A Beginner's Guide to oil drilling equipment in the oil and gas industry". [Online]. [Visited on 07/06/2023].

[11]. Pavel Talalay. "Design and Experiment of Clamper Used in Antarctic Subglacial Bedrock Drilling". Journal of Marine Science and Engineering, 2019. [Online].

[12]. Drilling manual. "Well Planning Overview". [Online]. [Visited on 02/06/2023].

[13]. The Ohio State University. "Crude oil commodity chain: Petroleum from the ground to our cars, Step 2: Drilling Extraction". [Online]. [Visited on 10/06/2023].

[14]. Wermac. "Wellhead and Christmas tree". [Online]. [Visited on 15/06/2023].

[15]. Drilling mentor: Making drillers for tomorrow. "Health, Safety And Environment In Drilling Industry". [Online]. [Visited on 15/06/2023].

[16]. Malik M. Ali Awan. "Drilling Measurements", 2022. [Online]. [Visited on 22/04/2023].

[17]. Prime horizontale. Mud Motors. [Online]. [Visited on 26/02/2023].

[18]. PowerPak Steerable Motor Handbook, Sugar Land, Texas: Schlumberger Educational Services, 2004. [Online]. [Visited on 26/02/2023].

Chapter 02

[1]. MIT Department of Civil and Environmental Engineering. "Design of Steel Structures", 1999.

[2]. David Poweleit & Raymond Monroe. "Steel Casting Mechanical Properties". Steel

Founders' Society of America, Crystal Lake, Illinois.
[3]. Heat Treating, Vol 4, Metals Handbook, American Society for Metals, 1991, 2173 pages. [Visited on 05/06/2023].
[4]. Said Bensaada. "Traitement thermique des aciers". [online]. [Visited on 29/05/2023].
[5]. William D. Callister, Jr. "Materials Science and Engineering: An Introduction" . John Wiley Sons, Inc. 2006, 975 pages. [Visited on 06/06/2023].
[6]. Lauralice C.F. Canale, L. Albano, George E. Totten, Lemmy Meekisho. "Hardenability of steel". University of Sao Paulo, School of Engineering of Sao Carlos, Brazil, [online]. [Visited on 23/06/2023].
[7]. Kamel Abadli. "Trempabilité des aciers".
[8]. arthur.boivin. "Notion de trempabilité". [online]. [Visited on 23/06/2023].
[9]. R.A. Grange. "Estimating the Hardenability of Carbon Steels". Metallurgical Transactions, 1973, Vol. 4, October, p.2231-2244. [Visited on 23/06/2023].
[10]. Aina Parasher. "Structural Steel". October 3rd, 2022. [Visited on 24/05/2023].
[11]. Osamah Sarhan, Mahdy Raslan. "Study of the elastic stiffness factor of steel structures with different lateral load resisting systems". International Journal of Advanced Engineering, Sciences and Applications (IJAESA). Volume 1, Issue 2, April 2020.
[12]. The Piping Mart. "Structural steel - Physical and chemical properties". [Visited on 25/05/2023].
[13]. Umiche, F.; Indacochea, J.; Wang, M.L. "Assessment of the Effect of Microstructure on the Magnetic Behavior of Structural Carbon Steels Using an Electromagnetic Sensor". J. Mater. Eng. Perform. 2008, 586–593. [Visited on 04/06/2023].
[14]. Welding Metallurgy. "Weldability of Structural Steels". [Visited on 23/063/2023].
[15]. Alhassan, M. and Bashiru, Y. "Carbon Equivalent Fundamentals in Evaluating the Weldability of Microalloy and Low Alloy Steels". World Journal of Engineering and Technology, 9, 782-792. [online]. [Visited on 23/06/2023].
[16]. Total Materia. The world's most comprehensive materials database. "Classification of carbon and low-alloy steels" [online]. [Visited on 03/07/2023].
[17]. Callister, Jr., William D., and David G. Rethwisch. Materials Science and Engineering: An Introduction. 10th ed., Wiley, 2021. Available at Materials engineering.

Chapter 03

[1]. Gwidon, W. Stachowiak. Wear Materials Mechanisms and Practice (pp21-22) [online]. Great Britain: edition, John Wiley Sons Ltd, May 2006. [PDF]. Wear Materials, Mechanisms and Practice
[2]. Kenneth G. Budinski. Guide to Friction, Wear, and Erosion Testing. (pp12) [online]. United States: Library of Congress Cataloging-in-Publication Data, (2007). [PDF]. Guide to friction, wear, and erosion testing
[3]. VectorStock. Friction rolling static and sliding vector [online]. Friction rolling static and

sliding vector
[4]. Said Bensaada and M.T. Bouziane. Tribologie, Principes et Matériaux (pp 105,115). [online]. Biskra, November 2019. [PDF]. TRIBOLOGIE, PRINCIPES ET MATERIAUX
[5]. Raymond G. Bayer, Tribology Consultant. Fundamentals of Wear Failures. [online]. Fundamentals of wear
[6]. Laboratoire Mateis. "Fretting corrosion and tribocorrosion". [online]. corrosion-fretting
[7]. Jean Dhers.Usure Avaris Corrosion: facteures de destruction des materiels industriels. edition : technique et vulgarisation. 1978. 190p.
[8]. Robert Scott. "Basic Wear Modes in Lubricated Systems".
[9]. Nawfel Muhammed Baqer Muhsin. Review on Corrosion and Rust Inhibition of Machines in Chemical Engineering Field Article. In: International Journal of Thermodynamics and Chemical Kinetics. review on corrosion
[10]. Harris, S. J. Overs, M. P. Gould, A. J. "The use of coatings to control fretting wear at ambient and elevated temperatures". [online]. Controlling fretting wear
[11]. Yongqing Fu, Jun Wei, Andrew W. Batchelor. "Some considerations on the mitigation of fretting damage by the application of surface-modification technologies". [online]. Mitigating fretting damage
[12]. Linn Efsing, Sara Olsson. Wear testing of high-alloy carbon steel used in mining tools [online]. Stockholm, Sweden: 2013. Wear testing of high-alloy carbon steel used in mining tools
[13]. G.W. Stachowiak, A.W. Bachelor. "Engineering Tribology". Fretting and minor wear mechanisms. (1992). 683-707. Engineering Tribology
[14]. Xu. Liqun. Abrasive wear of ferrous alloys [online]. Doctor of Philosophy thesis: Department of Materials Engineering. University of Wollongong. 1991. "Abrasive wear of ferrous alloys"
[15]. J. Paulo Davim. Mechanical and Industrial Engineering: Historical Aspects and Future Directions [online]. London: 01 December 2021. Mechanical and Industrial Engineering
[16]. Vakis AI et al.Modeling and simulation in tribology across scales: an overview[online]. TribolInt2018, [viewed 30 Mai 2023]125:169–199.
[17]. Nanova tribometers and lab services.About tribology [online].[viewed 30 Mai 2023].
[18]. Cheng Zhang and Pu Li.Repetitive Impact Wear Behaviors of the Tempered 25Cr3Mo2NiWV Fe-Based Steel.[online].26 January 2020.[Visited on 30/05/2023].

Chapter 05

[1]. Steel ss. "Data Table for:Carbon steel:SAE 9314". [online]. [visited on 01/07/2023]. available at https://www.steelss.com/Carbon-steel/sae-9314.html
[2]. Online Metals. "alloy steel 9310 product guide". [online]. [visited on 01/07/2023]. available at https://www.onlinemetals.com/en/product-guide/alloy/9310
[3]. Raju Prathipati. Siva Prasad Dora. Wear behavior of wire electric discharge machined

surface of 316L stainless steel. [on line]. [viewed 25/06/2023].
[4]. Taekyung Lee. Tribological and corrosion behaviors of warmand hot-rolled Ti-13Nb-13Zr alloys in simulated body fluid conditions. [on line]. [viewed 25/06/2023].